ABSTRACT

BARBOUR, SPENCER ANDREW. Surface Modification of Polyester Films with Electrically Conductive Carbon Nanotube Sheets. (Under the direction of Dr. Philip Bradford).

Due to their unique electrical, thermal, and mechanical properties, carbon nanotubes (CNTs) provide a potential alternative to traditional transparent conducting films such as indium tin oxide (ITO). While most current research in this field involves carbon nanotube films produced via dispersed solutions or solvents, highly aligned spinnable CNTs present the potential for simpler production methods that could scaled up for industry. In this project, a continuous calendering process was developed to incorporate CNT sheets drawn from highly aligned, spinnable multi-wall arrays into the surface of a glycol modified polyethylene terephthalate (PETG) film. The process was optimized to achieve a high level of embedding which improved the electrical properties of the films. It was shown that by altering the growth parameters of the CNTs, the electrical and optical properties of the produced films could be controlled to a certain degree. Wiping the surface of the films with an ethanol soaked cloth removed any unembedded or insufficiently embedded CNTs which improved the transparency at the cost of increased the sheet resistance. A post production acid treatment reduced the sheet resistance without significantly affecting the transparency. Sheet resistances as low as 286 Ω/square were obtained at a transmittance of 42.55% at 550nm. A transparency of 65.83% was achieved at a sheet resistance of 1921 Ω/square. Various microscopy and spectroscopy techniques were used to analyze the film morphologies and better understand the mechanisms of the electrical, optical, and mechanical properties of the films. The flexibility of the films and potential applications such as strain sensing and electrically induced heating were also demonstrated. This process is a viable method for

producing continuous, semi-transparent, and electrically conductive CNT films. The process is versatile and can be altered to accommodate various polymer films. With further research in the area of CNT growth parameters and consistency, it is possible that these films could meet the standards set by ITO.

Surface Modification of Polyester Films with Electrically Conductive Carbon Nanotube Sheets

by
Spencer Andrew Barbour

A thesis submitted to the Graduate Faculty of
North Carolina State University
in partial fulfillment of the
requirements for the degree of
Master of Science

Textile Engineering

Raleigh, North Carolina

2014

APPROVED BY:

Dr. Russell Gorga

Dr. Yuntian Zhu

Dr. Philip Bradford
Chair of Advisory Committee

BIOGRAPHY

Spencer Andrew Barbour was born in Raleigh, North Carolina on December 13, 1989. After graduating from Southeast Raleigh Magnet High School in 2008, he enrolled at North Carolina State University to pursue a degree in Textile Engineering. During his undergraduate career, he interned at Cotton Incorporated and Bennett Aerospace where he gained valuable experience in the textile industry. Upon graduating, he began working as a supervisor at Nan Ya Plastics in Lake City, South Carolina where he was responsible for the production of partially oriented polyester yarn. In January 2013, he returned to North Carolina State University to pursue his Master's degree in Textile Engineering, working under the advisory of Dr. Philip Bradford. The project involved developing a process to produce carbon nanotube films and is sponsored by Eastman Chemical Company.

ACKNOWLEDGMENTS

To begin, I would like to sincerely thank Dr. Philip Bradford for his guidance and support throughout my graduate career. Attending graduate school was always my goal and I could not have asked for a better situation than the one I have been in for the past two years. Thank you to my awesome group for being so supportive and helpful. Kelly, Ozkan, James, Ang, Shaya, Karim, Jincheng, Kun, and Brian, I couldn't have asked for a better group of people to spend my days with.

I would also like to thank Eastman Chemical Company for sponsoring this research and providing the funding to make it possible. Thank you to Eastman employees Dr. Wayne Shih and Dr. Damon Billodeaux for being very informative and helpful throughout this project. You were both always very receptive to my questions and your activity and interest in the project really pushed me to succeed.

I would like to thank Kelly Stano, who was always willing to take the time out of her schedule to perform SEM for me and answer any questions I had. Thank you to James and Ozkan for showing me the ropes and guiding me through the CNT growth process. Thank you to Ang Li for performing the piezoresistive strain testing on my samples and to Mangesh Champhekar for taking the time to perform nanoindentation for me. I would also like to thank Chuck Mooney, Roberto Garcia, Yang Liu, Toby Tung, Birgit Andersen, and Judy Elson for helping me analyze my samples with various microscopy techniques. Another thanks goes to Dr. Gregory Parsons for allowing me to use his four point probe.

Special thanks to Dr. Russell Gorga, my undergraduate advisor and member of my committee, for being one of the best professors I ever had. You are the reason I really became interested in textile engineering. Thanks to you and your various demonstrations with rubber bands, plastic bags, and bouncy balls, I can confidently explain polymers to my non-textile friends and family. I would also like to thank Dr. Yuntian Zhu for serving on my committee.

Finally, I would like to thank my mom, dad, sister, grandma, Aunt Sue, and my fiancée Rose. Thank you mom for always pushing me to do my best in school and in life. Thank you all for being so supportive of me throughout this process. I couldn't have done it without you all.

TABLE OF CONTENTS

LIST OF TABLES

LIST OF FIGURES

1 Introduction

With the ever growing demand within the consumer electronics market, research in the area of alternative conductive materials has become more important and will continue to increase. ITO is the most commonly used material for applications that require high transparency and low sheet resistance such as liquid crystal displays, flat panel displays, plasma displays, touch panels, and solar cells. Although ITO dominates the market, there are drawbacks. Indium is a rare earth metal with a volatile market that presents risk to manufacturers. ITO is relatively inflexible and thus the electrical properties suffer upon bending. Deposition of ITO on substrates is also difficult and expensive, as it is usually deposited in a process that requires vacuum.. Due to their unique electrical, thermal, and mechanical properties, CNTs have been a key focus of widespread research to develop alternatives to ITO.

While most research has focused on producing semi-transparent conductive films with CNTs through dispersion methods such as filtration, dip coating, and air brushing, the relatively recent discovery of highly aligned, spinnable CNT arrays has opened the door for new processing methods. The ability to draw an aligned sheet directly from the array allows for simpler methods that can directly incorporate the CNTs into polymer films. Throughout this research project, a continuous calendering process was developed to directly incorporate the drawn CNT sheets into a polymer film using only heat and pressure. This process is introduced and optimized in Chapter 4. A post processing wiping method was also introduced to remove any unembedded or insufficiently embedded CNTs from the surface of the film which increased transparency at the cost of increased sheet resistance. Chapter 5 explores methods by which to control and improve the properties of the produced films. Once the process was optimized, it was necessary to look into the CNT production parameters since the CNTs are the driving force for the electrical and optical properties of the films. By adjusting the growth parameters to alter the height and diameter of the CNTs, the properties of the films could be changed. Although double wall CNTs are ideal for their combination of electrical and optical properties, our current growth process is unable to produce CNTs with so few walls. The benefit of our growth process is the ability to grow millimeter tall arrays which provide long pathways and many contacts points for electrons to travel along the CNTs. Microscopy and spectrophotometry were performed to analyze the morphology of the films and provide insight into the mechanisms behind the resulting electrical, optical, and mechanical properties.

Chapter 5 also demonstrates an acid treatment which can be used to decrease the sheet resistance of the CNTs through p-type doping without affecting the transparency. The simple post production process is beneficial in improving the properties of the produced films. Tests were also performed to demonstrate potential applications for the films such as piezoresistive strain sensing and electrically induced heating. The initial results from these tests were promising, however further research must be done in the area of CNT growth to improve the uniformity, consistency between growth runs, and the properties of the grown arrays to fully realize to the potential for these semi-transparent, electrically conductive films.

2 Literature Review

2.1 Carbon Nanotubes

2.1.1 Carbon Nanotube Properties

Although their discovery has been debated [1], there is no doubt that Ijima's work in 1991 [2] greatly increased scientific interest in carbon nanotubes. Carbon nanotubes have become focus of much research due to their unique mechanical, chemical, electrical and optical properties. Due to these unique properties, carbon nanotubes have many potential applications in the areas of sensors, reinforcement, energy storage, and conducting panels and films to name a few.

The basis of carbon nanotubes, the carbon atom, has an electron configuration of $1s^2$ $2s^2$ $2p^2$ in its free state. To form covalent bonds between atoms, one of the 2s electrons is promoted to 2p. Depending on where covalent bonding occurs, various allotropes of carbon such as diamond, graphite, and amorphous carbon can form. In graphite, a 2s electron is promoted to the 2p orbital and hybridizes to form three sp^2 orbitals, leaving one unhybridized p orbital. Graphite can be visualized as layered sheets of carbon atoms covalently bonded together in hexagonal patterns with a carbon-carbon bond length of 0.142 nm [3]. Each carbon atom has one free electron which forms delocalized planes on either side of the plane of their carbon atom. These free electrons are able to move between parallel planes a thus give graphite its electrical and thermal conductivity. Because the electrons can move between parallel planes but not adjacent planes, the electrical and thermal properties are anisotropic.

Carbon nanotubes are comprised of sheets of graphite rolled into a seamless tubular structure with a hollow center. A tube consisting of a single sheet of graphite, also known as graphene, is referred to as a single walled carbon nanotube (SWCNT). Two sheets of graphene rolled concentrically are called double wall carbon nanotubes (DWCNTs) and by adding more than two layers results in multi-walled carbon nanotubes (MWCNTs). When forming a carbon nanotube, the way in which the graphite layer is wrapped, known as the chirality, affects the resulting properties. The chirality is represented by integers (n,m) which indicate the number of unit vectors in two directions within the structure of the graphitic layer with the chiral vector being defined as $C_h = na_1 + ma_2$ where $n \geq m$ [3]. Depending on the values of n and m, the symmetry of the carbon nanotube structure will differ. If $n = m$, the CNT is referred to as "armchair" and if $n > 0$, $m = 0$, the CNT is called "zig-zag". All other integer combinations are called "chiral." Figure 2.1 provides a visual representation of these structures. The chirality affects the electrical properties of the CNTs. with armchair being metallic and zig-zag and chiral being semiconducting [4]. The chirality applies to a single wall, thus making it easier to determine for SWCNTs. For MWCNTs, there are multiple walls with differing chiralities which create a mixture of metallic and semiconducting properties.

The physical properties of CNTs are affected by the structure, number of walls, diameter and presence of defects. A wide range of moduli from 0.5 to 5.5 TPa have been predicted from simulations whereas experimental data shows the range to be 0.27 to 1.8 TPa [5]. The reason for the high variation of predicted data is the researchers must make an assumption about the wall thickness. The commonly accepted value of 0.34nm for the wall thickness yielded values around 1 TPa, whereas some authors chose much smaller values which resulted in higher predicted moduli.

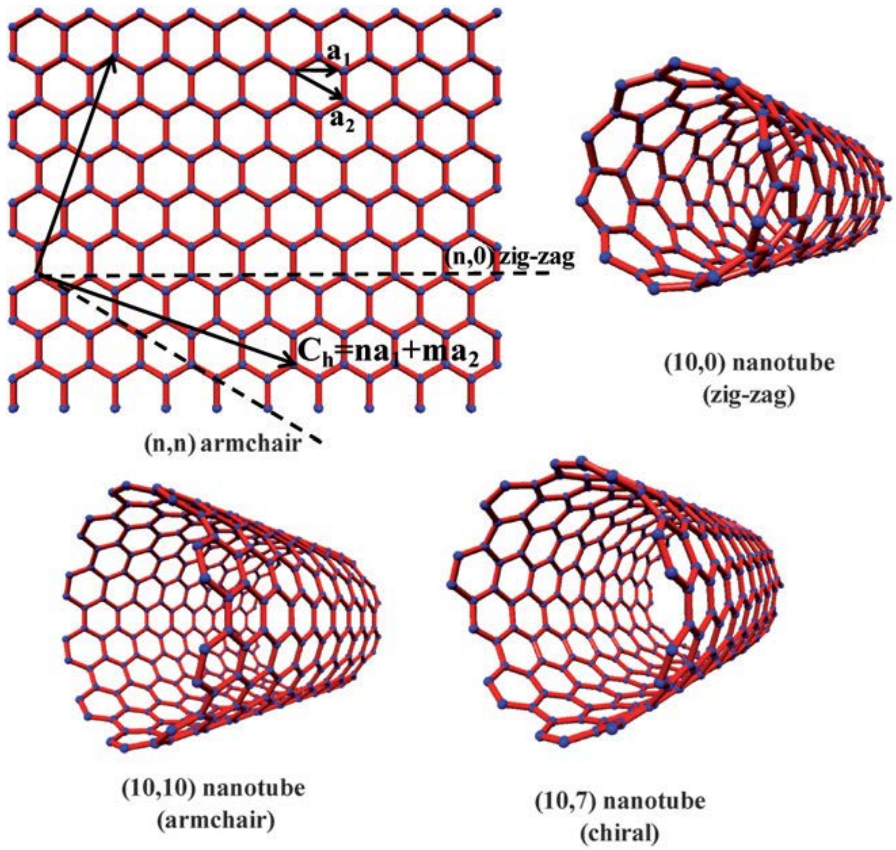

Figure 2.1 Schematic representation of the unit vectors of graphitic layer (a1 and a2) and various structures [6].

.

The electrical properties of carbon nanotubes are also anisotropic due to reasons previously discussed regarding graphite. Along the length of CNTs, ballistic conduction is exhibited. MWCNTs pose a different scenario perpendicular to the tubes due to electrons having to travel between the walls. A study by Li et al. [7] showed that MWCNTs exhibit quasi-ballistic electron transport behavior in MWCNTs which allowed the CNTs to carry large current at low bias voltage. This behavior is beneficial for the mass production of CNT conductive films because MWCNTs can be produced more easily and in larger quantities than SWCNTs and DWCNTs.

2.1.2 Carbon Nanotube Synthesis

There are many known methods for growing carbon nanotubes, however the three most common are arc discharge [8], laser ablation [9], and chemical vapor deposition (CVD) [10]. Although arc discharge and laser ablation methods produce consistent nanotubes with few to no defects, they cannot produce a large quantity of nanotubes. CVD, which was the method used to grow CNTs for this research, is able to produce large quantities of CNTs, however the consistency is lower and the number of defects is higher compared to CNTs produced by arc discharge and laser ablation. Although the quality of the CNTs is lower than other methods, utilizing CVD is a more economically viable option for large scale CNT production. A typical CVD setup includes a chamber in which the substrate can be held. This chamber is heated and gases are able to flow into the chamber. Figure 2.2 shows a typical thermal CVD setup with a quartz tube as the chamber. Within the CVD chamber, it is crucial to have precise temperature control along the tube.

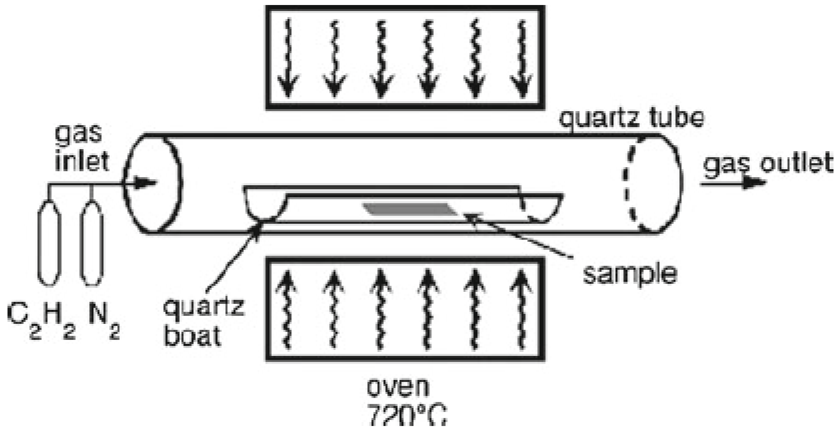

Figure 2.2 Typical chemical vapor deposition reactor set up for growing carbon nanotubes [3].

Although CVD has been used to produce carbon filaments since the 1960s [11], it was not until 1993 that a CVD method was modified to produce CNTs, using acetylene as the feedstock and Fe as the catalyst [12]. While there are many parameters than can vary between CVD processes, the basic steps remain the same. First the catalyst, usually a metal such as Fe, Ni, or Co), is deposited on a substrate. Upon heating to a certain temperature, a hydrocarbon gas is flowed. At this temperature, the catalyst restructures into nanoparticles and the hydrocarbon decomposes. The carbon species then dissolves into the metal and upon reaching the solubility limit, the dissolved carbon and grows from the catalyst particle in the form of a tubular structure [13]. Fe, Ni, and Co are generally the most effective metals in CVD of CNTs. It is believed that these metals are effective due to their catalytic activity in decomposing carbon compounds, their formation of metastable carbides, and the ability of carbon to quickly diffuse through them [14]. The catalyst compound is a key part of the CNT growth process and keeping them active is important in growing longer CNTs. A 2004 study by Hata et al. [15] determined that introducing water vapor in the growth process helps improve catalyst lifetime. The water is an oxidizer that removes amorphous carbon that would otherwise coat the catalyst particles and reduce their lifetime. This will become more apparent as the growth models of CNTs are discussed later in the section.

Common precursors used for CVD grown CNTs are acetylene [16], ethylene [17], methane [18], and ethanol [19]. It has been shown that the molecular structure of the precursor affects the CNT structure. Generally straight CNTs are produced by linear hydrocarbons such as acetylene and ethylene because at growth temperatures they decompose into linear carbon dimers and trimers [20]. Precursors consisting of cyclic hydrocarbons produce CNTs with many bends along their tube axis [21]. Because the precursor is a vital part of CNT growth, research is continuously being performed to improve the lifetime of catalyst for improved growth.

There are two widely used models for the growth of CNTs: base growth and tip growth. In the base growth model, the metal catalyst has a large contact angle with the substrate which does not allow the precipitated carbon to push the metal away from the substrate. Because the metal particle cannot be pushed up, the carbon precipitates out of the particle, which serves as the base for the CNT [22]. Conversely, in the tip growth method, the metal particle forms a small angle with the substrate. As the carbon precipitates from the metal particle, it is able to be pushed upward away from the substrate and continues to grow from the top until excess carbon caps the metal particle [23]. These two growth models are illustrated in Figure 2.3.

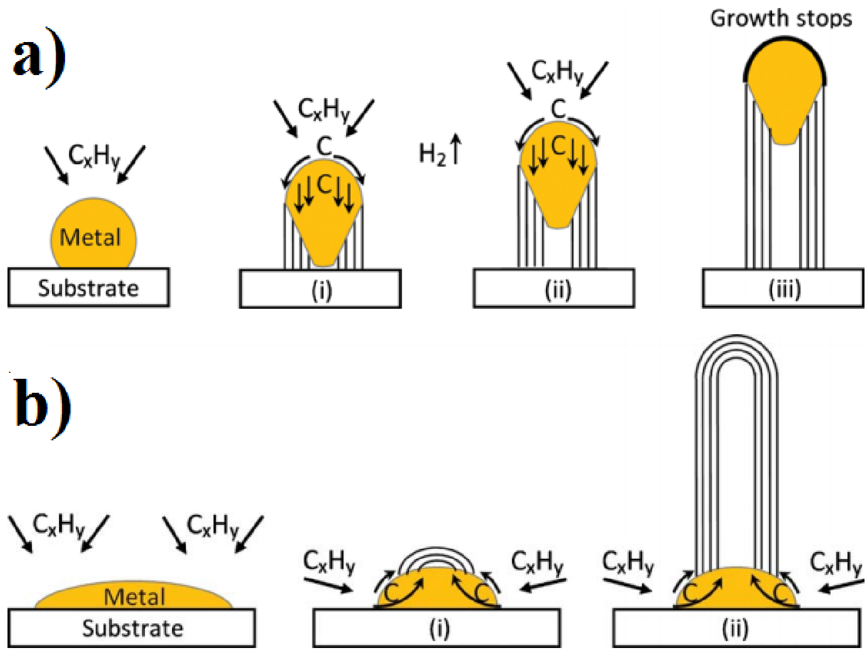

Figure 2.3 CNT growth models a) tip growth model and b) base growth model [20].

As carbon nanotubes break into more markets, the demand will continue to grow. CVD is currently the best method for production in terms of simplicity and quantity. Because of this, more research must be conducted in all areas of CVD growth of CNTs including equipment, precursors, catalysts, and growth mechanisms in order to improve growth rates, CNT lengths, and overall uniformity.

2.1.3 Vertically Aligned Spinnable Carbon Nanotubes

An intriguing aspect of vertically aligned CNTs is that when grown under the right conditions, they can be drawn from the array as fibers to form a thin sheet or can be twisted into a yarn. [24-30]. This characteristic provides a new and interesting range of applications for carbon nanotubes.

Spinnable CNT arrays are grown by CVD and because there are many variables involved in the sensitive process, few research groups can achieve spinnability with their arrays. Variables such as temperature, catalyst, hydrocarbon source, carrier and reactant gas flow rates and ratio, growth time, and substrate can all have an effect on the resulting spinnability of a grown array [31]. In order for the CNTs to pull from the array into a sheet, they must have very clean surfaces which allows for strong Van der Waals interactions with surrounding CNTs [32]. The Van der Waals interactions allow the CNTs to support one another and assemble into an aligned structure [33]. A model of the spinning process can be seen in Figure 2.4.

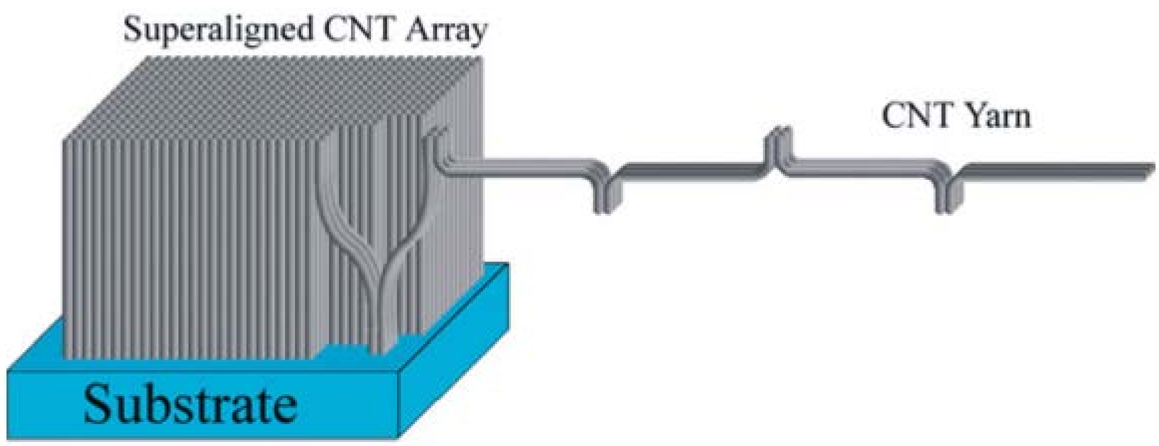

Figure 2.4 Model of continuously drawing CNTs from a vertically aligned array [32].

When the full width of CNTs from the array are pulled, they generally remain parallel and form a continuous sheet. Spinnable CNT arrays are beneficial in that they can form a network for materials in a simple manner without needing to be dispersed in a solution which can degrade the final product properties due to contamination and CNT breakage from sonication. Spinnable CNT arrays can be drawn into a thin sheet or twisted into a yarn. The spinnability of CNT arrays presents interesting possibilities due to the high strength and light weight of the drawn sheets and yarns. Directly spun CNT yarns have exhibited strengths in the range of 1.35 to 3.3 GPa and stiffnesses in the range of 100 to 263 GPa [28]. CNT sheets have markedly lower mechanical properties than yarns with a strength of 7.9 MPa and a modulus of 310 MPa being reported by Pohls et al. [34]. This study also explored the electrical properties of MWCNT sheets and reported the expected semiconducting nature with electrical conductivities of around 20 S cm^{-1}. CNT sheets can be drawn at 30 m/min and research has shown that a 1cm length of CNTs at a height of 0.245mm can produce 3m of drawn CNT sheet. The drawn CNT sheets also exhibit very low volumetric density (1.5 kg/m^3) and good sheet resistance (500 ohms/square). [35].

Although theoretically the drawn CNT sheets should be very aligned, they generally are not. As shown in Figure 2.5, this misalignment is a key contributor to the lower properties compared to individual CNTs and spun CNT yarns. The misalignment of CNTs within the sheet can function as a defect which yields lower mechanical properties. The misalignment generally proves to be beneficial for electrical properties. More contact points create more paths for electrons to travel throughout the sheet. This has been shown by Wei et al. through comparing the properties of drawn CNT sheets before and after shrinking [36]. Within the sheet, the electrical properties may be lowered due to high defect concentration [37] which causes localization of electrons. The electrical properties may also decrease due to the interfacial resistance between individual MWCNTs [38]. It has also been shown that longer CNTs produce more bundles within sheets than shorter CNTs [26]. While the presence of bundles improves the electrical properties of CNT sheets, they also decrease the degree of polarization and optical transparency. Polarization is affected because electron transport within the bundles creates random electric field radiation which interrupts the polarization caused by electron transport along the CNTs and reduces the degree of polarization. The presence of more bundles also decreases the optical transparency of the sheet. Bundling of CNTs causes more light to be absorbed by the sheet compared to a perfectly aligned sheet with no bundles or crossover points.

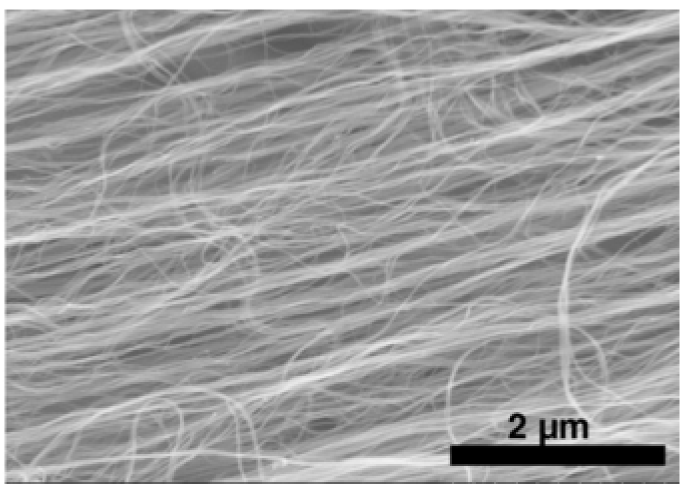

Figure 2.5 Scanning electron microscopy image showing misalignment within a drawn CNT sheet [34].

Vertically aligned spinnable CNTs provide an interesting new avenue for potential macro scale CNT applications. Although many advancements have been made in this area, more research must be conducted to enable the widespread availability of spinnable CNT arrays. We are able to alter growth parameters to achieve different mechanical, electrical and optical properties depending on the desired application. The unique properties of spinnable CNTs could yield new products that can be industrially produced through easier and cheaper methods than the current commonly used dispersion and solution routes.

2.2 Electrically Conductive Films

2.2.1 Transparent Conducting Oxides

Transparent electrically conductive films are important to many applications such as touch screens, solar cells, liquid crystal displays, and organic light emitting diodes [39]. The most widely used materials on the market in this area are transparent conducting oxides (TCOs). Since the production of the first TCO, cadmium oxide, by Badeker in 1907 [40] interest in these materials has grown greatly. Within the field of TCOs, the currently most common oxide that is commercially available is indium tin oxide (ITO). ITO is popular due to its low sheet resistance and high transparency. Typical ITO films will have sheet resistances less than 11 ohms/square with transparencies above 80% [41]. This combination of properties makes ITO an excellent choice for applications such as touch panels, liquid crystal and plasma displays, solar cells, and energy efficient windows. With the increasing market for electronic display devices such as mobile phones and televisions, the demand for TCOs has increased dramatically. Because the performance demands have also increased as the display sizes become larger and the data transfer speeds improve, research is continuously being performed to improve the electrical properties of TCOs while maintaining the optical transparency. Although ITO is the market leader, the continuous research in this field has yielded many different transparent conducting oxides with various advantages and disadvantages. Table 2.1 displays a range of properties and the associated oxides of choice.

Table 2.1 Optimum transparent conducting oxides based on various properties [42]

Property	Material
Highest transparency	$ZnO:F$, Cd_2SnO_4
Highest conductivity	$In_2O_3:Sn$
Lowest plasma frequency	$SnO_2:F$, $ZnO:F$
Highest plasma frequency	Ag, TiN, $In_2O_3:Sn$
Highest work function, best contact to p-Si	$SnO_2:F$, $ZnSnO_3$
Lowest work function, best contact to n-Si	$ZnO:F$
Best thermal stability	$SnO_2:F$, TiN, Cd_2SnO_4
Best mechanical durability	TiN, $SnO_2:F$
Best chemical durability	$SnO_2:F$
Easiest to etch	$ZnO:F$, TiN
Best resistance to H plasmas	$ZnO:F$
Lowest deposition temperature	$In_2O_3:Sn$, $ZnO:B$, Ag
Least toxic	$ZnO:F$, $SnO_2:F$
Lowest cost	$SnO_2:F$

Within the field of TCOs, there are two types of semiconductors: n-type and p-type. Most commercial TCOs that are produced from binary compounds such as SnO_2, In_2O_3, and ZnO or ternary compounds such as ITO function as n-type semiconductors [43]. N-type conductive oxides are typically used for TCOs due to their superior combination of electrical and optical properties compared to p-type [44]. N-type semiconductors, where the "n" stands for negative, are a class of doped semiconducting materials in which electrons are the majority carrier and electron holes are the minority carrier. The surplus of electrons creates an overall negative charge. These semiconductors are created by taking an intrinsic semiconductor and adding a dopant with donor impurities, which are atoms with more valence electrons than those that they replace. The extra valence electrons are then donated to the conduction band which creates a larger concentration of electrons compared to holes. Conversely, p-type semiconductors, where "p" stands for positive, involve doping an intrinsic semiconductor with acceptor impurities that accept valence electrons from the conduction band. This creates a greater concentration of electron holes and thus the holes are the majority carrier and the electrons are the minority carrier. Figure 2.6 shows the energy band diagrams for n-type and p-type semiconductors. From this we can see that the high concentration of electrons in the conduction band for n-type semiconductors causes the Fermi level to increase and lie closer to the conduction band. Alternately, the higher concentration of electron holes for p-type semiconductors causes the Fermi level to decrease and lie closer to the valence band.

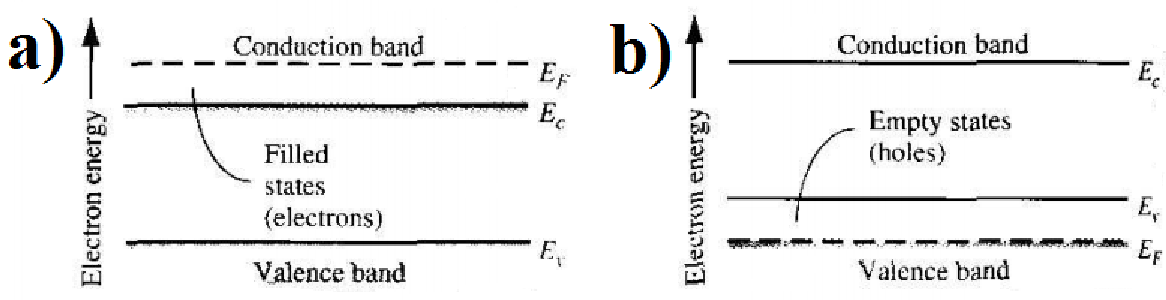

Figure 2.6 Energy band diagrams for a) n-type and b) p-type semiconductors [45].

When choosing a material for a TCO, it is important to select an oxide with a wide band gap (typically > 3 eV) and the ability to be doped to degeneracy [46]. The wide band gap allows for high optical transparency in the visible region and the capability to be heavily doped yields low electrical resistance. ITO fits these criteria very well with high dopability and a band gap of 4 eV [47].

ITO is typically produced via various forms of sputtering [48-51] but can also be produced through methods such as CVD [52-54], pulsed laser deposition (PLD) [55-57], and sol-gel processes [58-60]. Table 2.2 shows various methods reported in literature with their resulting electrical and optical properties. The figure of merit displayed in the table comes from the equation developed by Haacke [61] which is useful in comparing transparent conducting films based on their electrical and optical properties:

$$\varphi_{TC} = \frac{T^{10}}{R_s}$$

Where T is the optical transmittance and R_s is the sheet resistance. A larger figure of merit is obviously preferred because high transmittance and low sheet resistance is the goal for transparent conductive films.

Table 2.2 Electrical and optical properties of ITO films produced by various methods.

Production Process	Film Thickness (nm)	Sheet Resistance (ohms/square)	Visible Transmittance (%)	φ_{TC} (ohms^{-1})	Reference
Diode Sputtering	600	11	80	9.76×10^{-3}	41
R.F. Magnetron Sputtering	800	5	85	3.94×10^{-2}	51
Sol-gel	250	60	93	8.07×10^{-3}	60
CVD	160	12.5	80	8.59×10^{-3}	52
PLD	300	3	84.7	6.33×10^{-2}	56

While ITO films contain the best combination of electrical and optical properties, there are several drawbacks. The major economic drawback of ITO is the rarity of indium as a natural resource within the earth's crust [62]. This has resulted in price volatility due to the unstable market caused by an unsteady supply of indium. ITO is also a brittle crystalline material that may fracture upon bending which poses problems for applications that require maintained conductivity upon flexing. With the market demand for transparent conductive films expected to continue to increase and more research going into flexible electronics, OLED lighting, and thin film photovoltaics [63] these issues with ITO pose a potential problem for the future. Because of this, research is ongoing in regards to alternatives for ITO. Specific areas being studied include various metal oxides [64], graphene [65], and carbon nanotubes.

2.2.2 Carbon Nanotube Electrically Conductive Films

Films incorporating CNTs for the purpose of electrical conductivity can be produced in multiple ways. In general, CNTs are incorporated through either a solution based process or a dry process. Solution based processes encompass at least two steps where the CNTs are dispersed in a liquid and then assembled into a randomly oriented network structure. Dry processes are more desirable for industrialization due to their simplicity and the need for fewer processing steps. Solution based processing of CNTs into a network structure was first reported in 1997 by Niu et al. [66] where the CNTs were dispersed in water and then reassembled into an entangled structure. A key challenge in CNT dispersion involves overcoming the Van der Waals forces between the CNTs that encourage agglomeration. In addition to dynamic mixing methods such as sonication, researchers have also introduced functional groups on the surface of the CNTs [67], utilized organic solvents [68], and introduced surfactants into the solutions [69, 70]. Of these various methods, surfactants have proven to be the most effective for producing transparent films from CNT solutions. Adding functional groups to CNT surfaces leads to the formation of covalent bonding which alters the conjugated sp^2 structure of the CNTs [71]. Furthermore, the common solvents used, N-Methyl-2-pyrriolidone (NMP) and N,N-dimethylformamide (DMF), are toxic which creates safety concerns for processing.

Solution based processes generally fall under three categories: filtration, dip coating, or airbrushing. In a study by Li et al. [72], the optoelectronic properties of CNT films produced by filtration and airbrushing methods were compared. This study found that airbrushing yielded slightly better optoelectronic properties than filtration. A possible explanation of these results can be drawn from the processes themselves. In the airbrushing method, the CNTs are dispersed in a solution but then sprayed onto the substrate. As the CNTs land on the flat substrate surface, they are generally remain within that plane and are able to for a well-connected random 2-D network. By filtration, the CNTs are affected by the flow direction of the dispersion and may not all lie in the same plane which reduces the number of connections between CNTs. Another study by Liu et al. [39] compared filtration, airbrushing, and dip coating and found dip coating to have the best optoelectronic performance. One explanation for the superior performance of dip coated films is that better CNT alignment is imparted through forces from the linear motion of dipping and the forces induced by evaporation. Table 2.3 shows the electrical and optical properties of films produced using these methods from the literature.

Table 2.3 Comparison of optoelectronic properties of CNT conductive films manufactured by various methods

Method	CNTs	Sheet Resistance (Ω/square)	Transmission at 550nm	Reference
Filtration	DWCNTs	83	79%	73
Filtration	SWCNTs	80	75%	74
Filtration	SWCNTs	30	70%	75
Filtration	MWCNTs	213	77%	76
Dip Coating	SWCNTs	80	80%	77
Airbrushing	SWCNTs	1000	90%	78

Most studies regarding these processes for producing transparent conductive films have utilized SWCNTs. SWCNTs possess better overall properties than MWCNTs due to their structure. As stated in section 2.1, CNTs with "armchair" chiralities are metallic while "zig-zag" and chiral CNTs are semiconducting. In a given array of CNTs, the electronic properties will vary because not all CNTs will have the same structure, however recent studies have exhibited the ability to successfully produce a high percentage of metallic SWCNTs [79, 80]. Because the chirality can vary between the walls of MWCNTs, the overall array exhibits semi-metallic behavior. The potential for metallic behavior of SWCNTs makes them more appealing for conductive films. Unfortunately, SWCNTs are more difficult to grow and require methods that cannot currently match the quantity of MWCNT synthesis. More economical methods have been introduced using vertically aligned spinnable CNTs. In the work that has been published, only MWCNTs have been able to produce continuous wide sheets drawn from the array. The ability to drawn continuous sheets from a CNT array, as shown in Figure 2.7, brings promise to continuous production of CNT transparent conductive films. Because few research groups are able to achieve spinnability of their arrays, there has not been widespread research in producing or incorporating these arrays into transparent conductive films. In addition to the potential for continuous processing, this new capability provides a few advantages over solution methods because the CNTs are highly aligned and agglomerations that occur while mixing in solutions are not a problem.

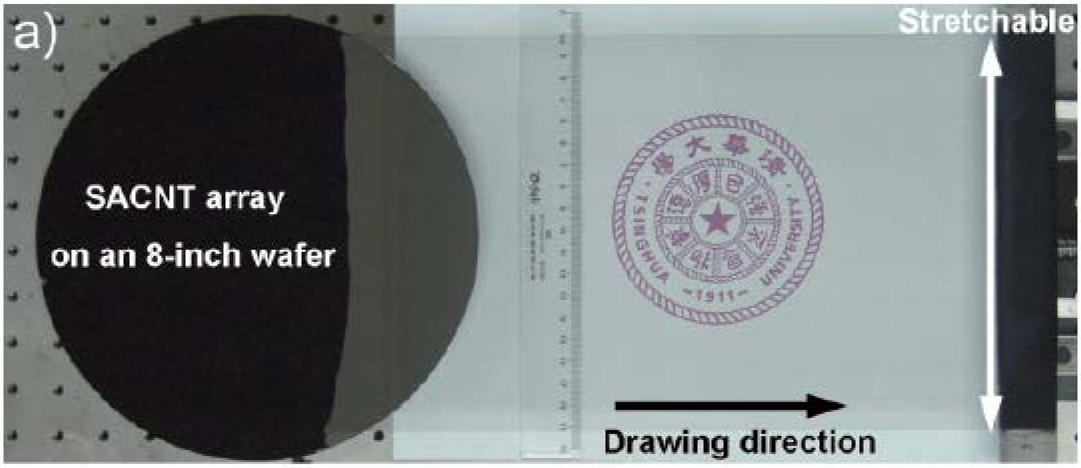

Figure 2.7 Wide semi-transparent sheet drawn from a spinnable vertically aligned MWCNT array [81].

In a study conducted by Lin et al. [82], sheets from spinnable MWCNT arrays were drawn and an electrodeposition process was used to deposit polyaniline (PANI) to form a composite film for use as a flexible, transparent supercapacitor. The addition of the conducting polymer, PANI, to the MWCNT sheet improved the specific capacitance significantly compared to pure PANI, the bare MWCNT sheet, and similar composite film of PANI and randomly dispersed CNTs. In another study by Di et al. [83], a simple method of winding a spinnable CNT sheet onto a rotating spindle was performed. Because many layers were wound, the resulting film was not transparent, however it did exhibit high strength and conductivity that was maintainable upon bending. This simple process shows steps toward a continuous method of creating transparent CNT conductive films.

Flexibility is a key component of CNT conductive films, as they can potentially find uses as flexible electronics for which ITO is not suitable. Through a continuous process of producing a conductive film from a spinnable array via a roll to roll process, Feng et al. [81]

showed that the electrical resistance upon flexing of their CNT/PET films was much more stable than that of ITO/PET. During the course of bending and coming to a conclusion as the films were folded, The CNT/PET film had a resistance increase of only 13% while the ITO/PET film had a resistance increase of 12708%. This is a very promising result that could lead to CNT conductive films meeting the needs of certain applications such as OLEDs, smart windows, and solar cells that may not require the conductivity and transparency on the level of ITO.

Some of the applications have already been demonstrated in the literature. The previously discussed study by Feng et al. produced a transparent touch panel using their CNT film made from spinnable MWCNTs and PET. These touch panels had transparency on par with similar ITO products and proved to be more durable after scrape tests. Li et al. [84] constructed an OLED using a flexible SWCNT/PET film for the anode. The resulting properties were acceptable, however still not on par with ITO. Although the properties were lower, the CNT film did provide good property stability upon flexing. Work is continuously being performed to improve the optoelectronic properties of these films. Solar cell anodes have also been constructed using MWCNTs [85] and SWCNTs [86]. Using SWCNTs, the solar cells performed similarly to ITO with comparable transparency. Although the electrical conductivity was not sufficient, the anodes showed superior properties upon bending compared to the ITO, which cracked and became insulating. Although CNT conductive films are in the early stages of research, these initial results and ensuing applications are promising for future prospects.

When analyzing the electrical and optical properties of CNT sheets, there is typically a tradeoff between the two. Longer CNTs will have more contact points which should improve the electrical properties by decreasing the overall contact resistance. Longer CNTs also produce more bundles than shorter CNTs which causes the sheet to absorb more light and thus the optical transparency decreases. Decreasing the electrical resistance and increasing the transparency will be an ongoing goal in this field. Because this is a relatively new field, much more research must be conducted to fully understand the mechanisms of spinnable CNT arrays in order to improve these properties. Variables such as growth parameters, CNT diameter, CNT height, and purity may all affect the spinnability and the ensuing optoelectronic properties of CNT sheets and films. The current results are promising and the intrigue of spinnable CNTs will promote more research to improve these properties in order to meet the needs of already established and also emerging markets for flexible, transparent electronics.

2.2.3 Characterization of Electrically Conductive Films

The most important properties of electrically conductive films are the sheet resistance, measured in ohms per square, and the transmittance, measured as a percentage. Achieving a combination of low sheet resistance and high transmittance is generally very desirable. For this reason, ITO is commonly used due to its superior combination of the two properties. There are multiple ways to measure sheet resistance, however a four point probe is the most common method. When using a four point probe, current is delivered to two of the probes and the voltage difference between the other two is measured. There are multiple terms that are often used to describe four point probe measurements such as sheet resistance, sheet resistivity, volume resistivity, bulk resistivity, surface resistance, and surface resistivity. Depending on the source, these terms can have different interpretations. When referring to electrically conductive films, sheet or surface resistances are typically measured in ohms per square whereas resistivities are measured in ohms-cm (or any other unit length). In 1954, L.B. Valdes used a linear four point probe method to measure resistivity of germanium transistors [87]. This work was later expanded on by Arthur Uhlir who looked at various geometries and the relationship between the resistivity, voltage, and current [88]. These studies focused on three dimensional materials and thus it can be concluded that the measurements being made were volume, or bulk, resistivities. Later, F.M. Smits defined a method by which to measure sheet, or surface, resistivities [89]. This work is applicable to thin films and materials in which electrically conductive layers have been deposited or embedded in the surface of an insulating material.

To determine the relationship between voltage, current, and sheet resistivity (which has also been referred to as sheet resistance for thin films), Smits begins with the logarithmic potential resulting from a current source in an infinite sheet:

$$\varphi - \varphi_0 = -\frac{I\rho_s}{2\pi}\ln r$$

where φ - φ_0 is the potential difference, I is the current, ρ_s is the sheet resistivity, and r is the distance from the current source. In a system with two current sources, one positive and one negative, a dipole is created which yields the following equation:

$$\varphi - \varphi_0 = \frac{I\rho_s}{2\pi}\ln\frac{r_1}{r_2}$$

In a four point probe configuration with equal spacing, current flows through two points and the voltage between the other two points is measured as shown in Figure 2.8 When applying the previous equation to a four point probe with equal spacing between each point, the potential difference is equal to the voltage, V, being measured between the inner probes and can be written as:

$$\varphi - \varphi_0 = \mathrm{V} = -\frac{\mathrm{I}\rho_s}{2\pi}\ln 2$$

Which can be rearranged and simplified to the commonly known equation for sheet resistance:

$$\rho_s = \frac{\mathrm{V}\pi}{\mathrm{I}\ln 2} = 4.5324\,\frac{\mathrm{V}}{\mathrm{I}}$$

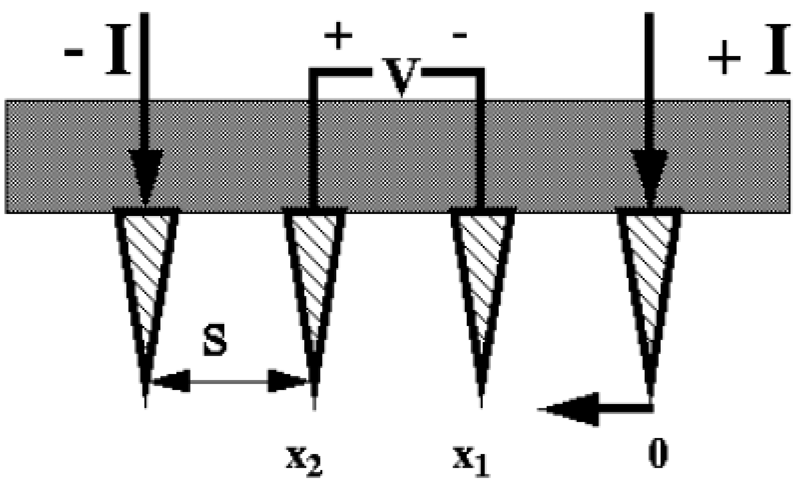

Figure 2.8 Linear four point probe configuration where current is delivered to the outer probes and the voltage difference is measured between the inner probes.

The previous equations all assume that the specimen being measured is of infinite size in all directions. Because this is never the case, there are correction factors for various sample dimensions. The correction factor, C, is incorporated into the sheet resistance equation as follows:

$$\rho_s = \frac{\pi}{\ln 2}\frac{V}{I}C$$

Geometric correction factors have been calculated for circular [90-92], semi and quarter circular [93], and rectangular shaped samples [94]. For the purpose of this study, only correction factors for thin (thickness < $\frac{s}{2}$) rectangular samples will be discussed. When analyzing rectangular geometric factors, the important dimensions are length, width, and probe spacing. Figure 2.9 depicts the dimensional sample setup and Table 2.4 shows the corresponding correction factors.

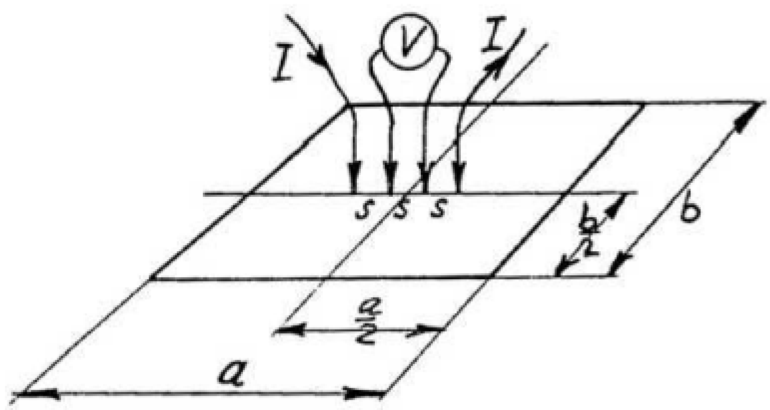

Figure 2.9 Rectangular dimensional setup for linear four point probe measurements [89].

Table 2.4 Four point probe correction factors for thin rectangular samples where a is the width and b is the length [94]

Rectangle b/s	a/b = 1	a/b = 2	a/b = 3	a/b ≥ 4
1.0			0.2204	0.2205
1.25			0.2751	0.2751
1.50		0.3263	0.3286	0.3286
1.75		0.3794	0.3803	0.3805
2.0		0.4292	0.4297	0.4297
2.5		0.5192	0.5194	0.5194
3.0	0.5422	0.5957	0.5958	0.5958
4.0	0.687	0.7115	0.7115	0.7115
5.0	0.7744	0.7887	0.7888	0.7888
7.5	0.8846	0.8905	0.8905	0.8905
10.0	0.9313	0.9345	0.9345	0.9345
15.0	0.9682	0.9696	0.9696	0.9696
20.0	0.9822	0.983	0.983	0.983
40.0	0.9955	0.9957	0.9957	0.9957
∞	1	1	1	1

2.3 Polymer Calendering

Calendering is a common method used to produce films and coated sheets of plastic and rubber materials. A calender is a simple system consisting of two rollers that rotate simultaneously and are usually heated to either melt a raw material or fuse two materials together. Additional roller can be added within the system if necessary. Although the capital investment is very high, calendering is usually preferred to extrusion because higher production rates with tighter tolerances can be attained. When calendering plastics, the polymer is generally heated prior to entering the calender. While still in the molten state, the polymer will pass through heated rollers which are set to the appropriate gap in order to achieve the correct film thickness. Cold rollers are then used to quench and solidify the semi-molten film. A typical calender system can be seen in Figure 2.10.

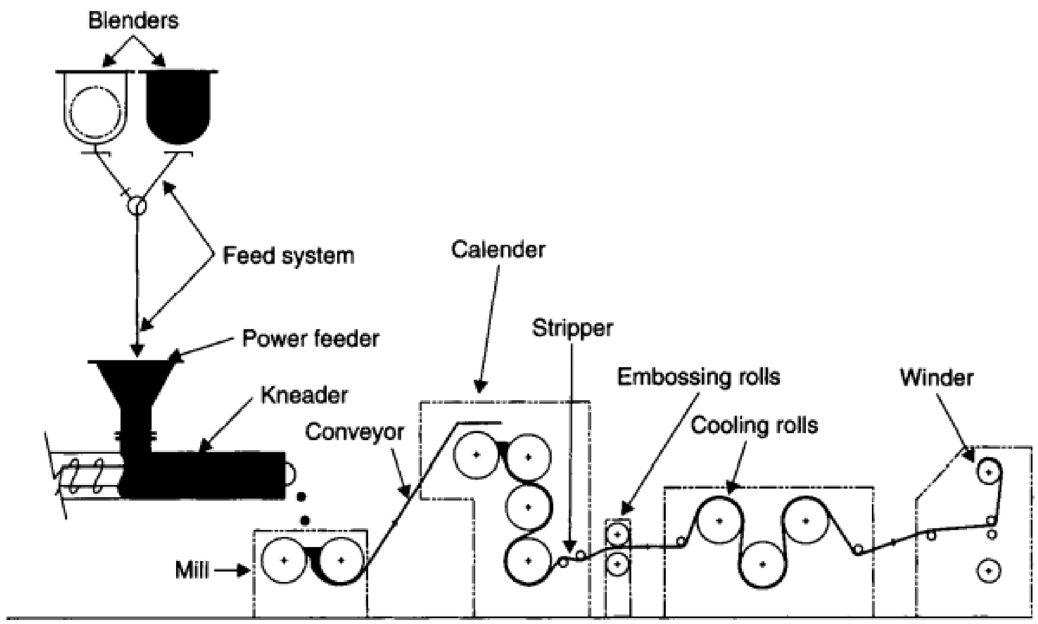

Figure 2.10 A typical multi-roller calender system used for producing films and sheets [95].

Calendering systems are also used for technical textiles such as airbag materials, breathable outdoor wear, filters for industrial and medical applications, parachute silk, packaging materials, and protective clothing [96]. Roll to roll processes involving calendering have also become promising in the area of electronic textiles as well [97, 98]. When producing electronic textiles via calender systems, the rollers are typically patterned to impart the desired circuit design in the surface of the film or fabric. The rollers can also be coated to transfer a conductive material such as a metal to the surface of the film or fabric.

An example of this process is depicted in Figure 2.11 where an organic material is first deposited on the film and then a metal layer is deposited. The textured roller then imparts a circuit pattern into the surface of the film and then the metal is etched away to complete the circuit.

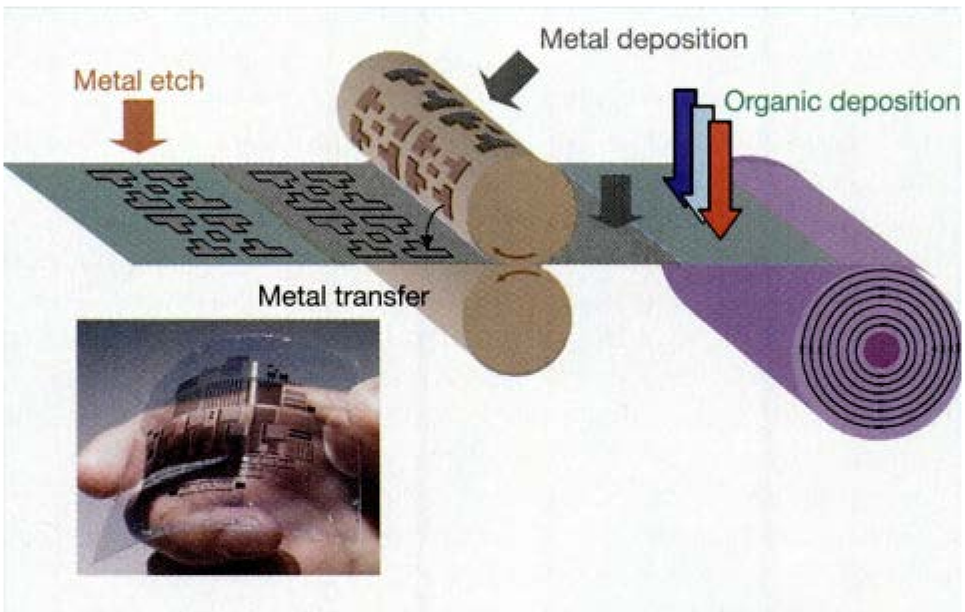

Figure 2.11 Calendering process for producing an electronic textile material [97].

In addition to being beneficial in producing electronic textiles, calenders have also been shown to improve the properties of printed electronic materials. A smooth surface is key for these materials and utilizing a calender can help reduce or create a more uniform surface roughness. In a study be Lee et al. [99], a calender was used to smooth a PET film printed with silver ink which resulted in a 10.2% average surface roughness decrease. Calendering was also shown to be beneficial in increasing the efficiency of TiO_2 films used as solar cells nearly as well as static pressing [100]. This is a promising finding because it could lead to dynamic processing of these materials which would greatly increase production rates.

Calendering has proven to be a beneficial production and post-production process for electronic textile fabrics and films. The ability to quickly produce these materials with a high degree of uniformity is a key gateway to mass production and lower product prices. As more research is conducted in the field of electronic textiles, calender systems should prove to be a major component for the industrialization of products.

3 Experimental

3.1 Materials

3.1.1 Spinnable MWCNT Array Synthesis

MWCNT spinnable arrays were produced using CVD. A flat quartz substrate and quartz tube were first burned at atmospheric pressure at 800°C and then etched in a diluted hydrofluoric acid bath for one to two hours to remove an contaminates. The quartz substrate was then placed on a stage within the quartz tube above a boat with 1g of $FeCl_2$ powder, which functions as the catalyst during growth. Prior to heating, the tube was loaded into the chamber and was vacuum pumped down to below 8 mTorr in order to remove any moisture or particulates from the system. Once the furnace pumped down to the appropriate pressure, the temperature was raised to 760°C. Upon reaching the set temperature, the gases were set to flow into the chamber. Two different gas setups were used during this project. Initially, 600 sccm of acetylene, 300 sccm of pure argon, and 100 sccm of argon/chlorine mixture (1.5% chlorine) was used. The argon/chlorine mixture became problematic and affected the spinnability of the grown CNT arrays. After analyzing the process using residual gas analysis, it became apparent that the argon/chlorine mixture was not consistent between growth runs as the chlorine concentration would vary. To solve this problem, a tank of pure chlorine gas was installed in place of the argon/chlorine mixed tank. With the new setup, 600 sccm of acetylene, 400 sccm of argon, and 1.5 sccm of chlorine was used. For both setups the pressure controller maintained a pressure of 3 Torr during growth.

Growth times were varied from 5 to 20 minutes to achieve different heights of the CNT arrays. Within the stated growth time range, the CNT height typically varied from 0.5

to 1.5 mm. After the arrays had grown for a given amount of time, the acetylene flow was turned off while the argon and chlorine flows remained constant. This process, which gives the CNT array its spinnability, is referred to as the post treatment because growth is terminated once the acetylene is no longer flowing to react with the catalyst. The post treatment proceeded for 20 minutes for each growth run.

After the post treatment, system was purged with pure argon for two minutes to flush out any remaining gases. The furnace was turned off and a fan was used to expedite the cooling process. Once the furnace reached 100°C, the system was closed off from the pump and argon was flowed to increase the pressure to atmosphere and allow the access door to open. The tube was then removed and cleaned. To analyze the spinnability, tweezers were used to draw the CNTs from the array. The spinnability was determined to be acceptable if a full sheet across the width of the array was able to be drawn and if the sheet could be maintained at drawing speeds of up to 0.5 m/min for processing. CNT arrays were grown for 5, 10, and 20 minutes with both the original growth setup (600 sccm acetylene, 300 sccm argon, 100 sccm argon/chlorine) and the pure chlorine setup (600 sccm acetylene, 400 sccm argon, 1.5 sccm chlorine).

3.1.2 PETG Film

The glycol-modified polyethylene terephthalate film (Eastar™ Copolyester 6763) was provided by Eastman Chemical Company. A second glycol, cyclohexanedimethanol (CHDM) was added which results in an amorphous polymer that will not crystallize. This allows for a wider range of processing parameters compared to polyesters that do crystallize.

The amorphous film was 4 mils (101.6 microns) thick with a glass transition temperature of approximately 85°C and a transmittance of 91% in the visible region.

3.2 Equipment

3.2.1 Platen Hot Press

Initially, a platen hot press was used to get a basic understanding of the parameters required and the interaction between the CNTs and the PETG film. The hot press used was custom built for the laboratory. The press has a manual pressure adjustment system with a corresponding gauge and heat controllers for the top and bottom plates. A water cooling system allows for faster cooling by flowing water through the plates.

3.2.2 Calender

A customized calendar was designed and ordered from DPM Solutions. The DPM-6000HT calendar contains two 4" diameter steel rollers which were hardened to 57RC and plated with electroless nickel to provide a smooth and durable surface. Each roller has width of 7" and a 750W heater cartridge which can operate safely up to 200°C. The temperature of each roller is controlled by an I3222 Omega temperature controller and is measured with a K type thermocouple. An Enerpac hydraulic pump is used to apply pressure to the rollers and the gap between the rollers can be set by a screw system. Figure 3.1 shows the calender system as well as a diagram depicting the internal components.

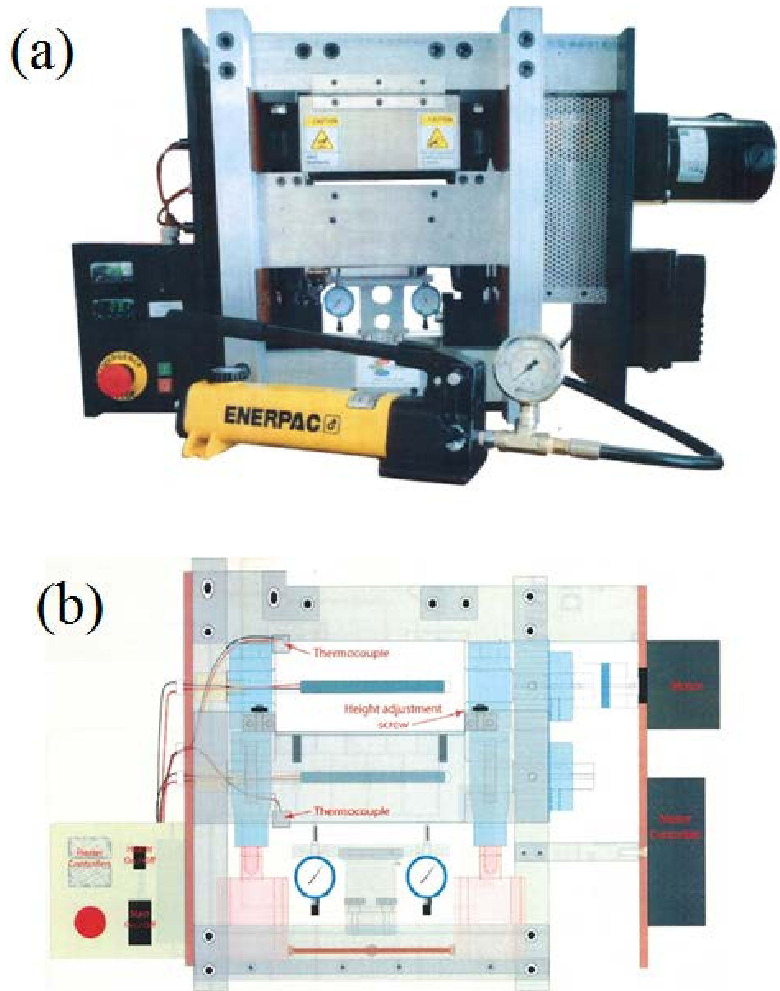

Figure 3.1 (a) Complete calender system and (b) diagram showing internal components.

The roller speed is adjustable from 0 to 6 rpm (0 to 2 m/min). The speed is adjustable by a dial on the side of the system. The dial is labeled with tick marks in increments of 10 from 0 to 100, however the rollers do not start rotating until the dial has reached 20. To simplify the speed determination for production, a tachometer was used to measure the speed at each incremental setting. Table 3.1 shows the corresponding speed at each setting.

Table 3.1 Dial settings of calender speed control system and corresponding roller speeds.

Dial Setting	Speed (m/min)
10	0
20	0.12
30	0.35
40	0.57
50	0.83
60	1.05
70	1.30
80	1.63
90	1.85
100	2.00

3.3 Equipment and Sample Production

3.3.1 Batch Heat Press Process

When making samples of CNTs embedded in PETG film using the heat press, first two polished steel plates were wiped with ethanol to remove any debris. Next, a 2" x 2" piece of PETG film was placed on one plate and the CNT sheet was pulled across with tape and carefully laid on top. The other polished plate was then carefully placed on top and a razor blade was used along the edge to cut the excess CNTs. Next, the plates were transferred to the heat press. This process is shown in Figure 3.2. After pressing and heating for a given amount of time, the system was cooled to below the glass transition temperature (approximately 80°C) of the PETG film using water, which flowed through hoses attached to the top and bottom plates of the heat press. The pressure was maintained during cooling because it was found that removing the pressure at elevated temperatures caused the PETG film to deform. The CNTs provided a buffer layer which prevented the top side from sticking to the steel plate even though the film was heated above the glass transition temperature. After cooling, the pressure was released and the plates were removed from the heat press. The plates were then carefully separated and if there was any sticking present, a plastic razor blade was used to remove the samples from the plate so as to not cause any scratches in the plate which could affect future samples.

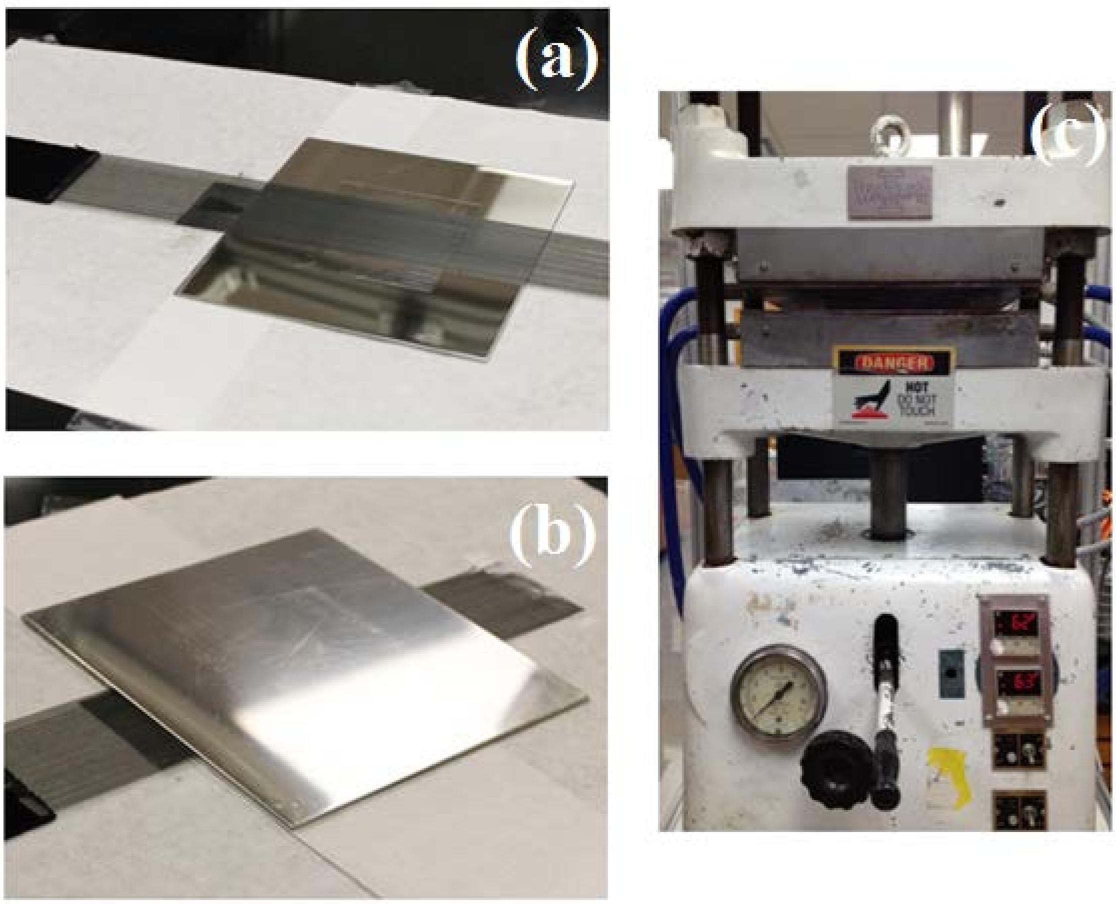

Figure 3.2 Process of producing batch samples of CNT embedded PETG films. (a) CNT sheet is pulled across PETG film on metal plate (b) Top plate is carefully placed (c) Plates are transferred to heat press.

3.3.2 Continuous Calender Process

Prior to receiving the calender, a custom enclosure was built. The aluminum enclosure was made with acrylic paneled access doors on all sides, an adjustable stage for the CNT arrays, an adjustable holder for the PETG film spool, and a variable speed take up roller was installed on the back side. The stage for the CNT arrays needed to be adjustable because the angle of CNTs being pulled from the array is important for processing. An angle too large resulted in too much upward force which pulled the array away from the substrate and caused problems during drawing. An angle too small caused the drawn CNT sheet to rub against the edge of the substrate which caused the sheet to snag and break apart. An optimal angle was between 10 - 20 degrees. Extruded aluminum bars were installed under an aluminum sheet to support the weight of the 200 pound calender. A ventilation system was installed on top of the enclosure to remove any airborne CNTs. The enclosure and the installed parts can be seen in Figure 3.3.

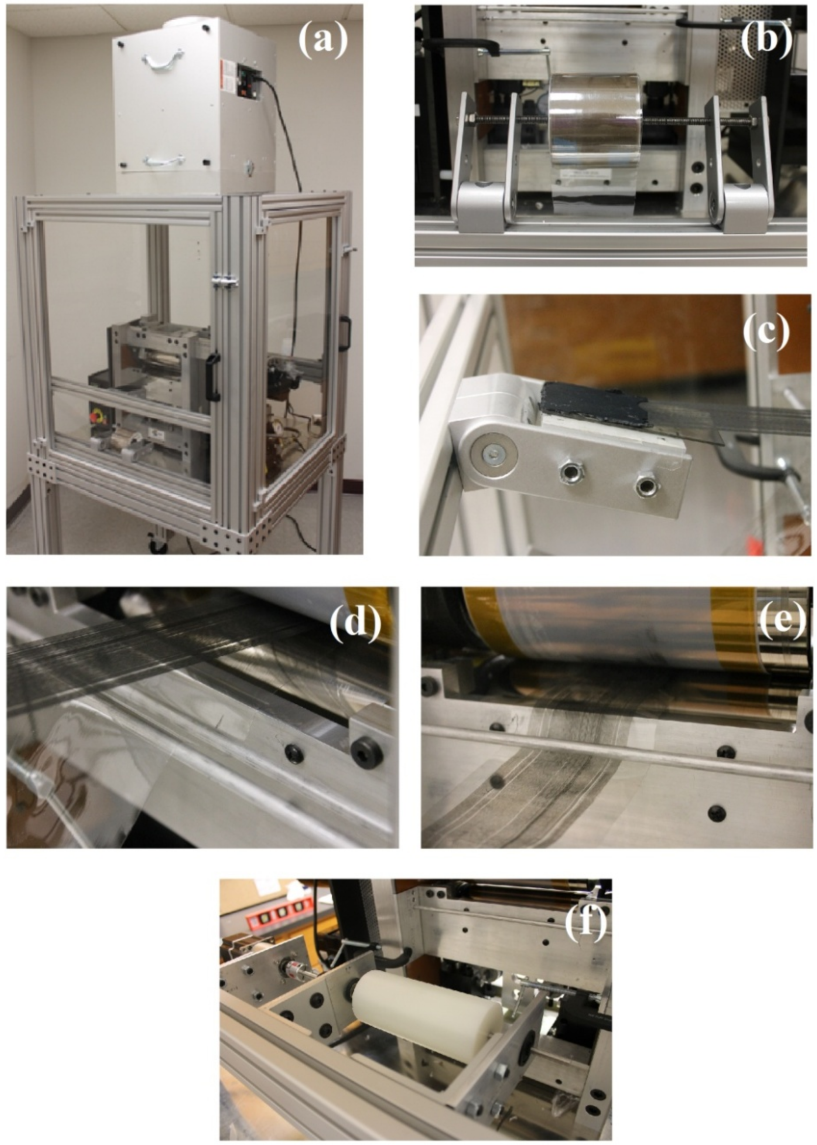

Figure 3.3 (a) Custom built enclosure with installed calender system (b) Adjustable holder for PETG film spool (c) Adjustable stage for CNT array (d) Tension rods at the entrance of the calender (e) Tension rod at exit of calender (f) Variable speed take up roller.

Upon receiving the custom built calender system, the processing variables had to be identified and optimized. The variables involved in the process were the roller temperatures, roller speed, roller gap, and take up speed. Because it was difficult to achieve perfect alignment between the CNT sheet and the PETG film, a slightly wider film was used to allow for processing to continue in the case that the alignment shifts. The CNT sheets were 2.5" wide whereas the PETG film was 3" wide. During testing, it was found that at higher temperatures the edges of the film without CNTs embedded would stick to the metal roller and cause deformities as the take up roller pulled the film away from the calender roller. To resolve this problem, adhesive backed Kapton and Teflon (2 mils thick) films were tested by adhering them to the calender roller. The Kapton film proved to be more durable than the Teflon, however the PETG film would stick to it along the outer edges causing deformities as it was taken up. The Teflon film prevented adhesion and allowed for a smooth release of the film from the roller, however durability was an issue. When the gap between the rollers was too small, the PETG film pressed into the Teflon and create indentations and wrinkles. A thicker Teflon film (10 mils) was ordered and applied which proved to be more durable than the 2 mils Teflon. Figure 3.4 shows the film exiting the calender with the uncovered electroless nickel plated roller, the Kapton covering, and the 10 mils thick Teflon covering. From these images it is clear that the Teflon covering was most suitable for the process as the film made a smooth exit and there was little to no adhesion of the film to the Teflon.

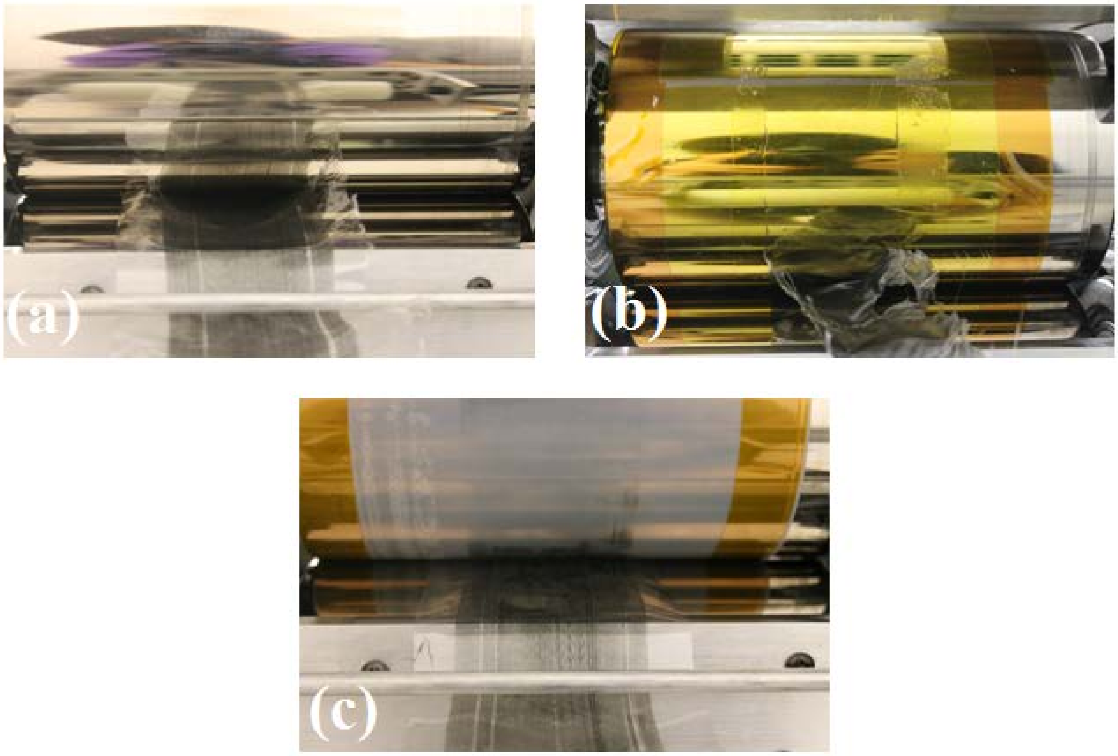

Figure 3.4 Calender exit uniformity with (a) no roller covering (b) Kapton covering and (c) Teflon covering.

3.3.3 Sample Handling

To determine the level of embedding, the samples were wiped after removal. It was found that wiping with an ethanol soaked cloth removed more CNTs than simply wiping with a dry cloth. The same effect was observed when using water in place of ethanol. The moisture allowed the wipe to make better surface contact with the sample and also provided capillary hydroscopic forces which both made the CNTs more likely to attach to the wipe and become removed from the surface of the film. Well embedded CNTs will not detach from the surface, however unembedded and some partially embedded CNTs will be removed. Wiping was found to increase both the transparency and sheet resistance of the films and may be necessary for certain applications where touching the surface is required and unwiped films may pose a health hazard due direct contact with CNTs. The samples were wiped carefully in a circular motion until it was apparent that no more CNTs could be removed. Figure 3.5 displays unwiped, dry wiped, and ethanol wiped samples on top of text to better depict the transparency of the films. From these images, it can be seen that wiping with a dry cloth removed some of the lose CNTs from the surface and the film became less hazy. A more significant difference can be seen with the ethanol wiped sample, where many of the bundles of unembedded CNTs were removed and the transparency noticeably increased.

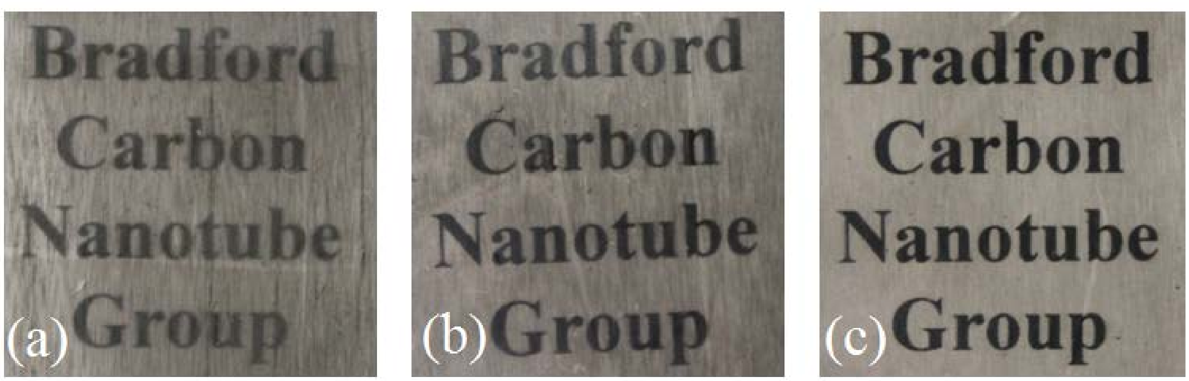

Figure 3.5 (a) Unwiped sample, (b) dry wiped sample, and (c) ethanol wiped sample.

3.4 Testing Procedures

3.4.1 Electrical Testing

The sheet resistance of the produced films was measured using a Jandel RM3-AR four point probe. The probes were aligned linearly with a 1mm spacing. In order to ensure accurate measurements with no edge effects, the measurements were taken towards the middle of each sample. 5 measurements were taken in each direction to get a good representation of the sheet resistance both parallel and perpendicular to the CNT alignment. Although rounded tips are preferred to prevent any penetration into the film, only pointed tips were available. The height of the probe was carefully adjusted to ensure good contact with the film but little to no penetration beneath the surface. In order to ensure consistency between measurements, the current was adjusted to obtain a voltage of 15 mV before the sheet resistance was recorded.

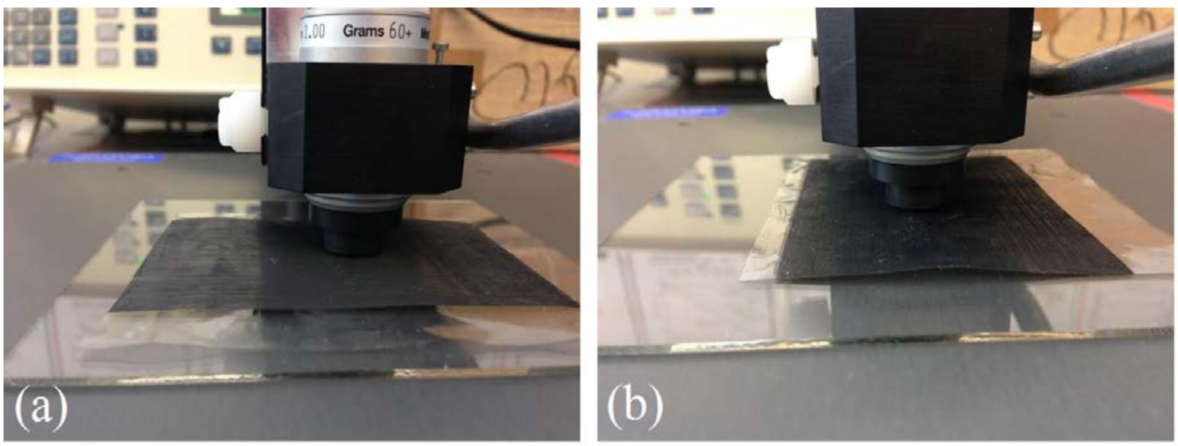

Figure 3.6 Four point probe measurement (a) parallel and (b) perpendicular to the CNT alignment direction.

For the electrical heating experiment in section 5.3.4, an Electro Industries Model DIGI 360 regulated DC power supply was used. The samples were cut to 1" x 2" and copper foil was used at each end to clamp the leads from the power supply. The voltage was increased in increments of 5V up to the maximum output of 30V. A Fluke thermometer was used with a k-type thermocouple placed on the surface of the CNT film to measure the temperature. At each voltage interval, the voltage was held until the temperature stabilized before recording.

Figure 3.7 Heater setup using a sample cut from the continuously produced CNT/PETG film. Leads connected using copper foil.

3.4.2 Spectroscopic Testing

Transmittance measurements were taken for each film using a Varian Cary 300 UV-Vis spectrophotometer. A 2 cm x 2 cm section was cut out of each sample and placed in the holder. Samples were tested in the wavelength range of 800-200 nm. The value at 550nm was reported which is standard for transparent conductive films because this value is in the middle of the visible range region. Three different areas were tested for each sample to achieve an average transmittance value.

To determine graphitic quality and defect density, Raman spectroscopy was performed on the CNT arrays using a Renishaw Ramascope with a laser wavelength of 514 nm. The laser spot was focused using a Renishaw microscope. The radiation was collected within a wavelength range of 1200 - 1800 cm^{-1}. After collecting the data, the G (1350 cm^{-1}) and D (1580 cm^{-1}) peaks were identified and used to calculate the G to D ratio for each CNT array.

3.4.3 Microscopy

Scanning electron microscopy (SEM) images were taken using a FEI Verios 460L. Samples were cut and attached to holders using carbon tape. The samples were then imaged, removed and wiped with ethanol, then imaged again to achieve a comparison between unwiped and wiped samples.

Transmission electron microscopy (TEM) images were taken using a JEOL 2010F. CNT samples were taken from each array and sonicated in ethanol for 30 minutes to achieve an adequate dispersion. Drops of the dispersion were then placed on C-Flat holey carbon grids produced by Protochips. Next, the grids were baked at 70°C to evaporate the ethanol and prepare them for imaging.

Atomic force microscopy (AFM) was performed using a Bruker D3000 Scanning Probe Microscope. Samples were first wiped with an ethanol soaked cloth to remove any unembedded CNTS from the surface. This step was necessary because testing samples without wiping to remove excess CNTs resulted in unclear images as the probe tip would get caught on the loose CNTs.

3.4.4 Mechanical Testing

Nanoindentation testing was performed using a Hysitron Triboindenter. A Berkovich tip with a 100 nm radius was used. Samples were cut to 2cm x 2cm and measurements were taken in 3 separate areas on each sample. Within each area, the load was varied from 50 to 450 µN in increments of 50 µN.

Strain tests were performed using a MTS Landmark Servohydraulic 250kN test system. The CNT films were cut to 25.4mm x 50.8mm and attached to the center fiber glass composite cut to dimensions of 300 mm × 30 mm × 6.35 mm using epoxy. The film was adhered with the CNT side facing the composite, so as to best reflect the behavior of the composite. The fiber glass composites were tabbed at the ends with 2 mm thick fiberglass sheets with a taper angle of 20°.Prior to attaching the CNT film, copper foil was adhered to the composite to function as electrodes at each end of the film. Lead wires were soldered to the exposed copper film. A metal foil strain gauge (Vishay Micro-Measurements 250LW) was mounted on the opposite surface of the composite substrate in order to measure the actual strain data and correlate it to the resistance change of the film. The monotonic tensile tests were performed with a fixed displacement rate of 1.5 mm/min during which the resistance data was recorded using an Agilent 34420A multimeter. The fiberglass composites were strained until failure. Figure 3.8 shows the set up of this test.

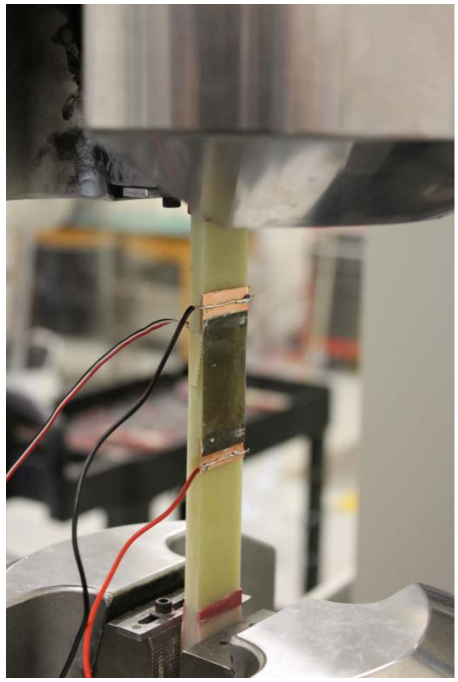

Figure 3.8 Monotonic tensile test set up showing the CNT film adhered to the fiberglass composite with leads connected at each end.

4 Optimization and Preliminary Results

4.1 Platen Hot Press Trials

Before the calender system was received, the platen hot press previously described was used to manufacture samples and get an understanding of the interactions of the PETG film and the CNTs under the presence of heat and pressure. Knowing that the glass transition temperature of the PETG film was 85°C, the trials were started at 90°C and increased in increments of 10°C up to 130°C. At 140°C, some melting of the film was observed which resulted in deformation and difficulty removing it from the plates. The maximum achievable pressure of 4000 psi was used to achieve the highest possible level of embedding and two samples were produced at each temperature. One set of samples was held under temperature and pressure for 1 minute before being cooled and the other set was held under temperature and pressure for 5 minutes before being cooled. The 1 minute samples were meant to simulate a quick exposure to the temperature like the calender system. Although the exposure time will be much less with the calender, exposure times of less than 1 minute in the heat press proved to show very little embedding. This is due to the presence of the steel plate between the film and the heat press. The heat must transfer through the steel plate which takes time. With the calender, there will be no buffer layer between the film and the heat source. The 5 minute trials were performed to ensure the film met the desired temperature for an extended amount of time to fully understand the effect of temperature on embedding. After production, the wiping method described in section 3.4 was utilized and thus each sample can be separated into three different categories: unwiped, dry wiped, and ethanol wiped. The unwiped samples were not modified and were characterized in their as-produced state. The dry wiped samples were wiped with a dry nonwoven cloth and the ethanol wiped samples were wiped with an ethanol soaked nonwoven cloth. Samples were wiped until it was apparent that no more unembedded CNTs could be removed from the surface. This was judged by initially wiping with one area of the cloth and then moving to a clean area of the cloth to determine if more CNTs could be removed. When the new area of the cloth was clean after wiping, the wiping was deemed sufficient. Figure 4.1 Shows the resulting sheet resistance parallel to the CNT alignment and transmission for the unwiped, dry wiped, and ethanol wiped samples.

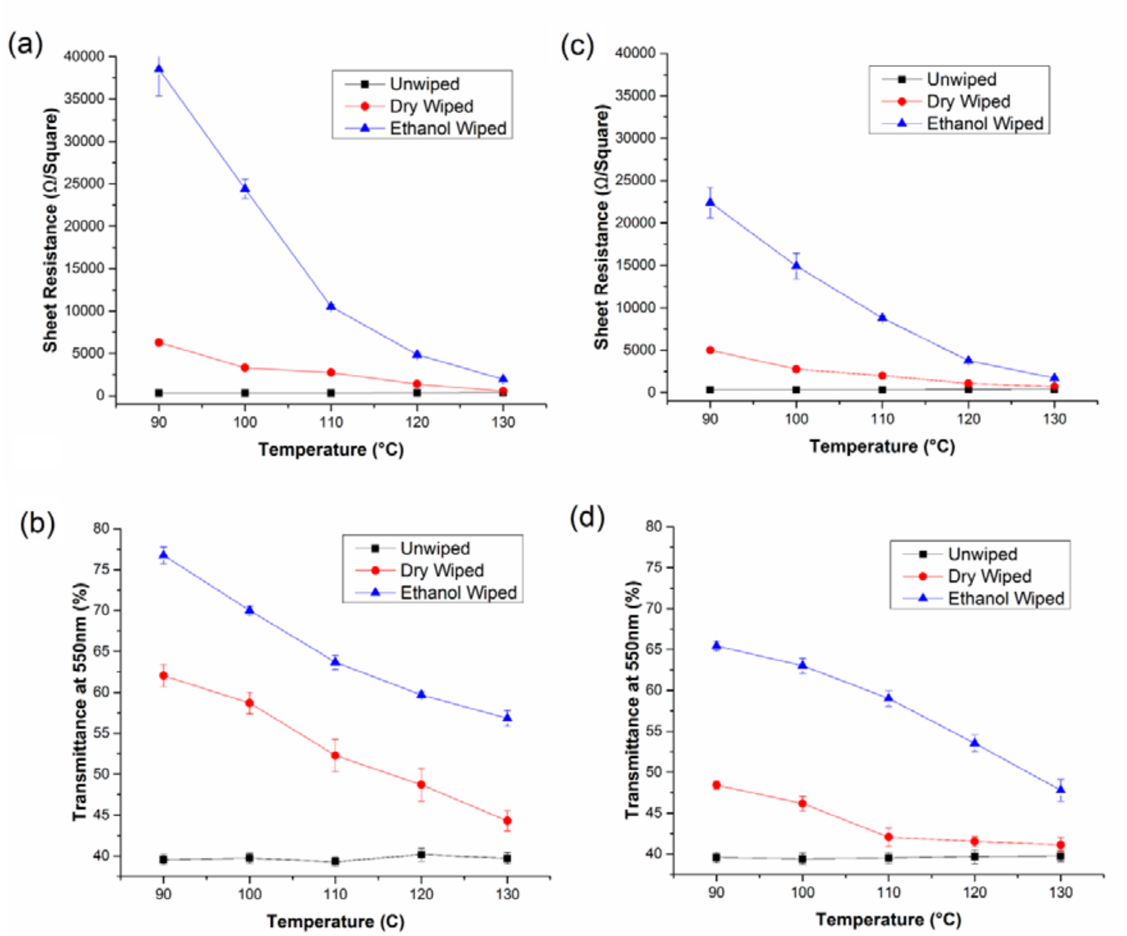

Figure 4.1 Comparison of sheet resistance in the parallel direction and transparency measurements for varying temperature for (a) and (b): 1 minute heat press samples and (c) and (d): 5 minute heat press samples.

From this data, the correlation between processing temperature, sheet resistance, and transmittance is clear. For the unwiped samples, the transmittance remained constants at around and 40% for all temperatures. Although it is not apparent in the graph due to the scale, the sheet resistance showed a slight increase (325 to 380 Ω/square) as the temperature increased. This increase can be explained by the higher level of embedding. The polymer film becomes softer at high temperatures and allows the CNT sheet to become further embedded which means there were less CNTs exposed on the surface of the film. As the temperature increased, the gap in sheet resistance and transmittance between the unwiped, dry wiped, and ethanol wiped films decreased. This further proves that the level of embedding improved as temperature increased, as few CNTs were able to be removed from the surface of the film.

In comparing the 1 minute and 5 minute samples, there is a noticeable difference between the wiped samples. Maintaining temperature and pressure in the heat press for 5 minutes allowed for a higher level of embedding which can be interpreted from the lower sheet resistance and transparency values compared to the 1 minute samples. Complete embedding could not be achieved even at 130°C. This could be the result of the steel plate not having a smooth enough surface, CNTs protruding in the z direction from the CNT sheet, or the presence of thicker CNT bundles. Complete embedding could be achieved at higher temperatures, however this was a result of melting and the resulting films became very distorted and difficult to remove from the plates.

The sheet resistance was also measured in the perpendicular direction to the CNT alignment. A slight increase was found from the parallel direction. For comparison purposes. Figure 4.2 displays the parallel and perpendicular sheet resistance of only the sample pressed at 130°C for 5 minutes. The reason for only a small increase between the parallel and perpendicular measurements is the small probe spacing. Sheet resistance measurements were made using another four point probe with a 5mm spacing and the difference between parallel and perpendicular directions was much greater. Although the CNTs have a general alignment in one direction, there are many crossover points within the sheet. The alignment may also be altered during processing and handling. With the small probe spacing used, the presence of crossover points and bundles makes a significant impact on the perpendicular measurements. With a larger spacing, the presence of these misalignments within the sheet should be less influential. Because the films are most likely to be used in the direction of the best possible electrical properties, only the parallel sheet resistances will be reported going forward.

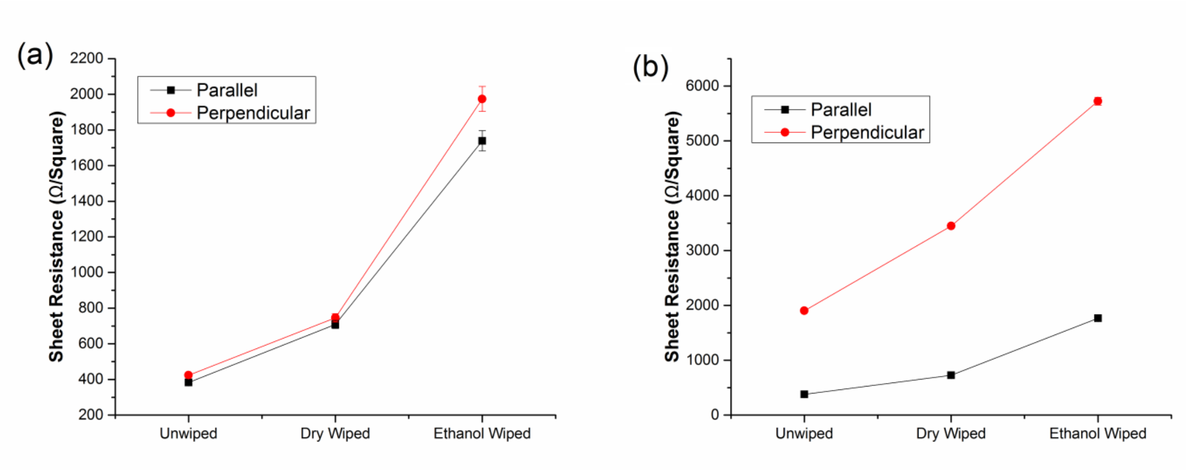

Figure 4.2 Comparison of sheet resistance parallel and perpendicular to the CNT alignment direction for a sample pressed at 130°C for 5 minutes using (a) 1mm probe spacing and (b) 5mm probe spacing.

Unfortunately an effective method of breaking the films and imaging to analyze the cross-section and level of embedding could not be achieved. Cryo ultramicrotome was performed on the samples, however the PETG film was unable to exhibit a brittle break and the shearing force of the knife skewed the CNTs which made determining the cross-section depth of the CNTs difficult. Focused ion beam SEM (FIBSEM) was also attempted to analyze the cross section of the samples. This method was also unsuccessful as the beam melted the film and the CNTs in the cut area and made determining the depth difficult. Images from these two processes can be seen in Figure 4.3.

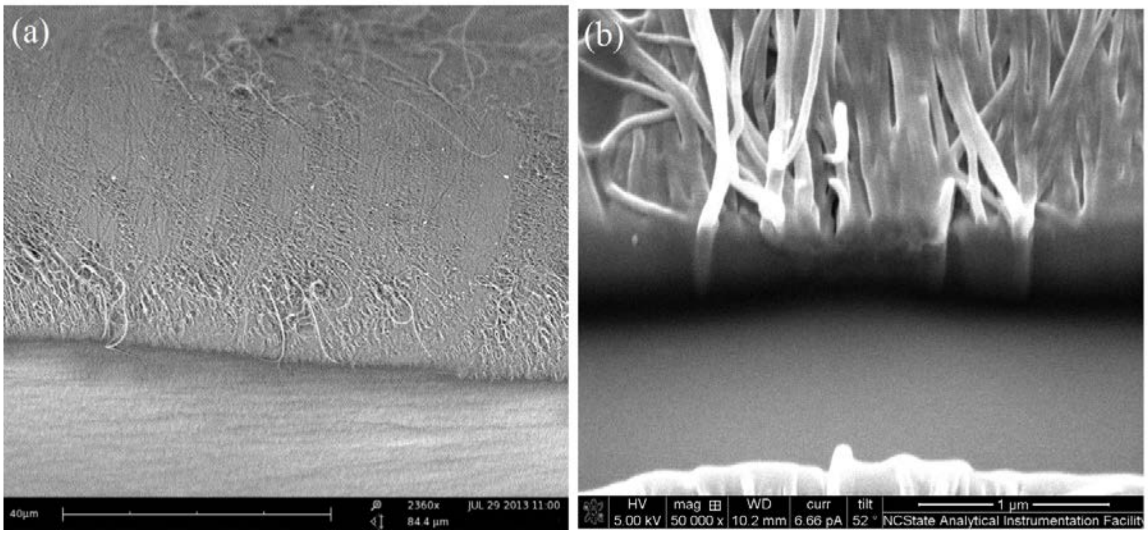

Figure 4.3 (a) Cross section image of a sample cut using cryo ultramicrotome and (b) cross section image of a sample using FIBSEM..

An alternative method of embedding the CNT sheet into the PETG film using a solvent instead of heat was also attempted. Tetrahydrofuran, a known solvent for PETG, was applied to the surface of the film using an adjustable spray gun attached to a nitrogen gas line. The film was sprayed to full coverage and then placed on a steel plate. The CNT sheet was then drawn across the film and another plate was placed on top. The plates were then placed in the heat press at room temperature and pressed at 4000 psi for 1 minute. Upon removal, it was apparent that the solvent created a tacky surface and did not yield a uniformly embedded sample. Because of this, the solvent embedding method was not explored further with the calender system. The solvent spray system and a sample can be seen in Figure 4.4.

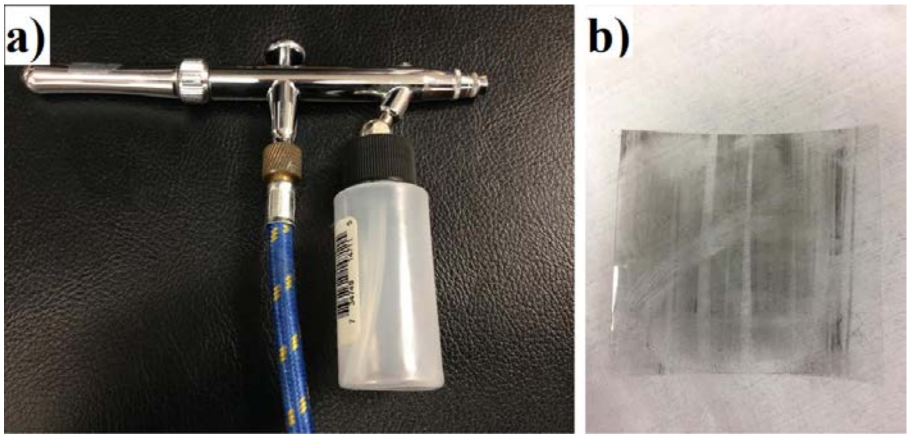

Figure 4.4 (a) Solvent spray system, (b) CNT-PETG film manufactured using solvent method.

4.2 Initial Calender Trials

After the custom built calender and the additional parts were installed, the proper gap, speed, and temperature had to be determined. The calender system is capable of speeds up to 2 m/min, however it was determined that roller speeds in excess of 0.83 m/min (2.6 rpm) resulted in processing problems. At higher speeds, the spinnability of the CNT array was compromised and gaps in the sheet would form which are not ideal for samples. The gaps also exposed the PETG film and caused it to stick to the roller. Having a complete sheet across the width of the array is important for producing samples that are conductive throughout. Gaps with no CNTs result in insulating areas of just PETG film within the samples. Furthermore, higher speeds often caused the PETG film to migrate across the width of the rollers. Although careful precautions were taken to ensure an even gap, proper tension, and good alignment, the migration proved to be unavoidable at high speeds. Because of these reasons, only speeds below 0.83 m/min were used for producing samples.

Because the PETG film is 4 mils (101.6 microns) thick, the gap between the rollers had to be less than that to provide compression of the film and allow for embedding of the CNT sheet. Gaps of 3.5 mils, 3 mils, and 2.5 mils were tested and it was found that a gap of 3 mils or less resulted in too much compression and the Teflon film being damaged. The damage to the Teflon film caused wrinkles and air bubbles to form which resulted in a non-uniform surface. This result can be seen in Figure 4.5.

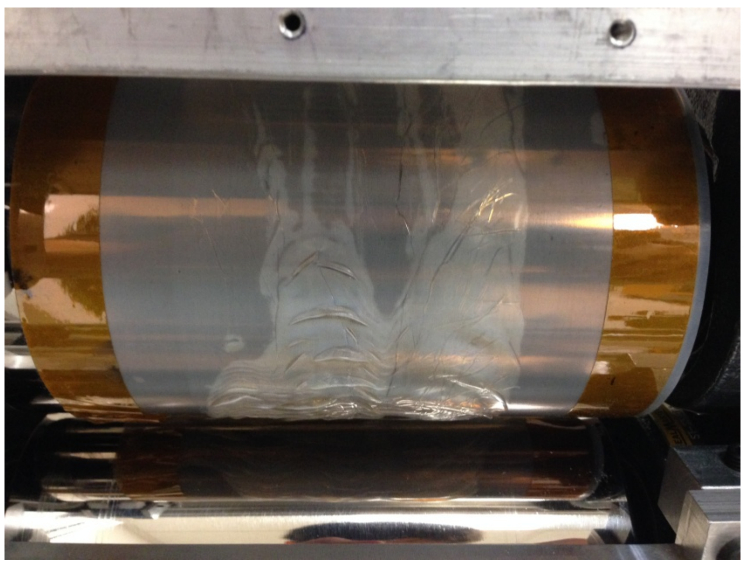

Figure 4.5 Wrinkling and loss of adhesion of Teflon roller cover caused by increased pressure.

To confirm the results from the previous heat press trials, samples were produced within the same temperature range using the calender system. With the upper limit of appropriate processing speed being 0.83 m/min, two samples were produced at each temperature: one sample at 0.83 m/min and another at 0.57 m/min. As a lab scale version of a potentially industrial process, faster speeds are more ideal for production. The effect of roller speed and temperature on the resulting sheet resistance and transmittance can be seen in Figure 4.6.

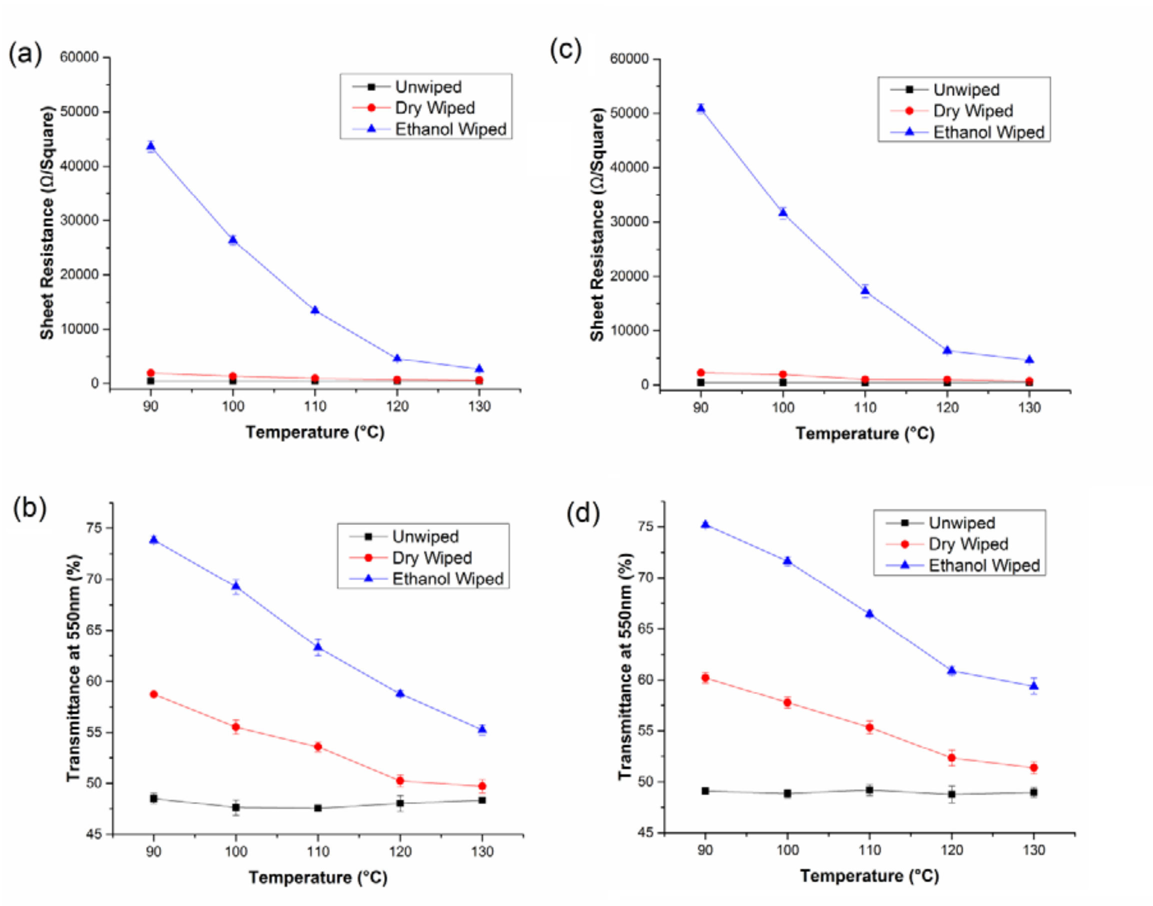

Figure 4.6 Comparison of sheet resistance and transparency measurements for varying temperature for (a) and (b): 0.83 m/min and (c) and (d): 0.57 m/min samples.

These results show a similar trend to what was reported with the heat press in the previous section. Increasing the temperature resulted in a decrease in sheet resistance and transmittance for the wiped films, while the unwiped samples remained constant. Processing at 0.57 m/min resulted in improved electrical properties over using a roller speed of 0.83 m/min. At 130°C, the average sheet resistances of the dry wiped samples for 0.57 m/min and 0.83 m/min were 596.2 and 707.8 Ω/square, respectively. A larger difference was seen between the ethanol wiped samples, which had sheet resistance values of 2608 and 4606 Ω/square. The decreased sheet resistance for the 0.57 m/min samples also resulted in a lower transmittance compared to the 0.83 m/min samples, with the average values of the 130°C ethanol wiped samples being 55.2% and 59.4% respectively. Two sample t-tests were performed to determine the significance of the results for the ethanol wiped samples produced at 130°C. The parameters and results of the t-tests can be seen in Table 4.1. Based on these tests, it was concluded that the sheet resistance of the 0.83 m/min samples was significantly greater than that of the 0.57 m/min sample. In regards to the transmittance, we were unable to conclude that the average value for the 0.83 m/min sample was significantly greater than that of the 0.57 m/min sample. The goal of any transparent conductive film is to have the lowest sheet resistance and highest transmittance possible. Because producing samples at the 0.57 m/min resulted a significantly lower sheet resistance without a significantly greater transmittance than samples produced at 0.87 m/min, a speed of 0.57 m/min was advantageous. A speed of 0.57 m/min was used for the proceeding experiments.

Table 4.1 Two sample t-tests performed on ethanol wiped samples produced at 130°C under speeds of 0.83 m/min and 0.57 m/min

	Sheet Resistance		Transmittance	
	0.83 m/min	**0.57 m/min**	**0.83 m/min**	**0.57 m/min**
Sample Size	5	5	3	3
Mean	4606	2608	59.4	55.2
S.D.	209.2	235.5	1.38	0.86
H_o	$\mu1 - \mu2 \leq 0$		$\mu1 - \mu2 \leq 0$	
H_a	$\mu1 - \mu2 > 0$		$\mu1 - \mu2 > 0$	
t*	14.18		0.09	
d.f.	8		4	
Rejection region for α = .05	t* > 1.860		t* > 2.132	
Conclusion	Reject H_o		Fail to reject H_o	

After achieving these results, samples were also produced at higher temperatures, with varying results. 140°C was attempted at the previously determined speed of 0.57 m/min, however at this temperature the PETG film became too soft and the tension imparted by the take up roller resulted in tearing and distortion. A film produced at this temperature can be seen in Figure 4.7. As discussed in the previous section with the heat press, processing at 140°C softened the film too much and may have caused significant creep of the film between the calender rollers and the take up roller. A processing temperature of 135°C was then attempted with more promising results. The film remained intact and did not distort due to the tension from the take up roller. Because the highest level of embedding possible is desired to enhance the electrical properties of the films, it was decided that 135°C would be used going forward.

Figure 4.7 Sample produced at 140°C exhibiting temperature induced deformation.

4.3 Conclusions

These initial trials suggest that embedding the CNT sheet into the PETG film was possible. Based on the experiments using the heat press, it was determined that a temperature of at least 130°C would be necessary for the calender process. In optimizing the calender process, it was found that complete embedding was not achievable while producing a dimensionally stable film due to the low residence time between the rollers. A Teflon roller cover proved to be beneficial in preventing the film from sticking to the roller and improving the uniformity of the film. Temperatures of 140°C and above caused the film to soften too much and the tension caused by the take up roller distorted the film. 135°C was deemed an appropriate temperature for achieving the highest level of embedding possible while maintaining the dimensional stability of the resulting film. By wiping the films with a dry or ethanol soaked clothes, unembedded CNTs were removed from the surface which improved the transparency but increased the sheet resistance. These two properties are inversely correlated and the main goal of all transparent conductive films is finding a balance between the two. Faster production speeds are desirable for mass production however in order to achieve the best possible level of embedding, a maximum speed of 0.57 m/min was used. Going forward, methods to improve the embedding level and alter the electrical and optical properties of the films will be explored.

5 Results and Discussion

5.1 Calender Production

After determining that 135°C and 0.57 m/min were the optimal temperature and speed combination for producing uniform, dimensionally stable films, the next step was to determine how to increase the level of embedding. As previously discussed, decreasing the gap between the rollers was not viable due to damage to the Teflon film. Another method explored was passing the film through the rollers multiple times. After undergoing the initial pass with the CNTs, the film was then taken off of the take up roller and sent through the calender again. This was performed up to five times. This method was successful and could be easily integrated into a manufacturing process by having multiple calenders in series with one another. The gap was slightly decreased for subsequent passes to account for compression in the film from the first pass. After producing each sample from one to five passes, the electrical and optical properties were measured. The results can be seen in Figure 5.1.

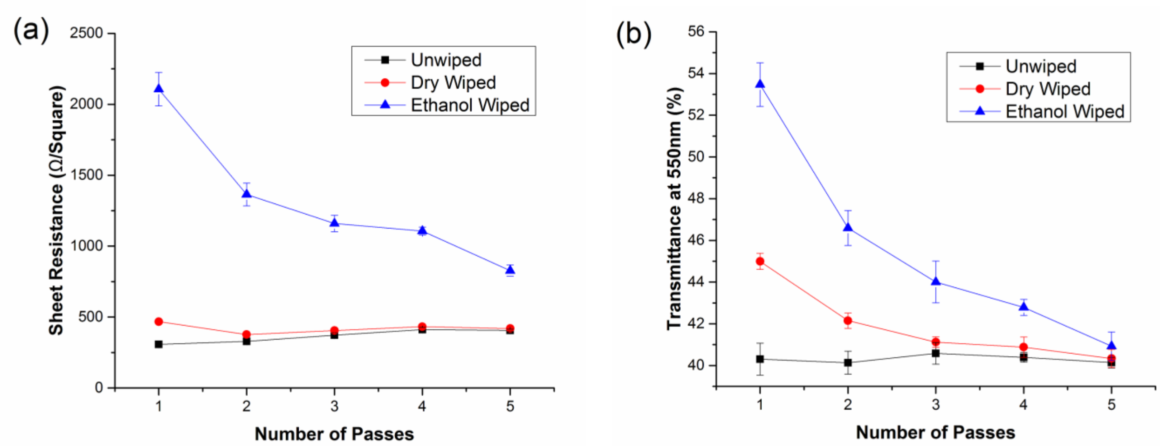

Figure 5.1 (a) Sheet resistance measurements and (b) Transmittance measurements obtained from samples produced with multiple passes through the calender.

To better visualize these results, a picture was taken of each sample with text in the background. As shown in Table 5.1, the transmittance increased as the wiping progressed for each sample. The unembedded large bundles of CNTs were removed which made the background text appear more clearly.

Table 5.1 Visuals of samples produced with multiple passes showing the progression of transmittance upon wiping

	Unwiped	Dry Wiped	Ethanol Wiped
1		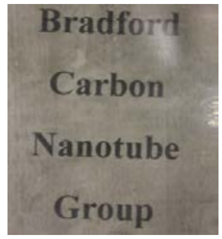	
2		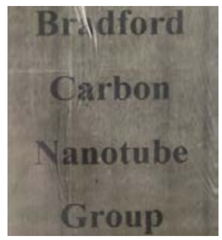	
3		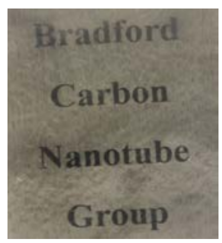	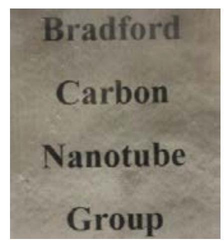
4			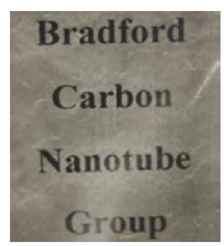
5			

These results show that both the sheet resistance and transmittance of the ethanol wiped sample decreased as the number of passes increased. Beginning at two passes, very few CNTs were able to be wiped away using a dry wipe, which is depicted in the data as there is little difference in sheet resistance and transmittance between the unwiped and dry wiped samples after two passes. This indicates there were more CNTs embedded well into the surface that were unable to be wiped away with an ethanol soaked wipe. After five passes, very few CNTs could be wiped off with ethanol, which is apparent from the only slight increase in transparency between the unwiped and ethanol wiped samples (36.8% to 37.3%). The sheet resistance demonstrated a more drastic increase (406 Ω/square to 827.6 Ω/square). SEM was used to further investigate the effect of multiple passes on the films. As shown in Figure 5.2, the five pass samples exhibited a greater level of embedding. It is apparent that there are fewer CNTs protruding from the surface after five passes and a greater concentration underneath the polymer. Ethanol wiping the sample after only one pass removed many CNTs from the surface and left areas of pure polymer film with no CNTs where the level of embedding was not sufficient and the CNTs were removed via wiping. This is a major reason for the drastic increase in sheet resistance and transmittance between the one pass unwiped and ethanol wiped samples. Furthermore, there are CNTs which were partially embedded that could not be removed by the wipe but were instead misdirected which decreased the level of alignment of CNTs within the film. This may have also been a contributing factor to the increased sheet resistance in the parallel direction. With the five pass unwiped sample, we can see that there is more misalignment compared to the one pass unwiped sample. This misalignment may be attributed to handling or could have been caused by the additional passes through the calender. Wiping the five pass sample with an ethanol soaked cloth removed significantly less CNTs than doing so after only one pass. A higher concentration of CNTs can be seen in the five pass ethanol wiped sample with better alignment, indicating there were fewer unembedded or partially embedded CNTs on the surface that could have been misaligned by the wiping process. Even after five passes, the CNT sheet was unable to be completely embedded. Additional passes were performed, however the film began to deteriorate and non-uniformity became an issue. Because the system only contains one set of rollers, the samples had to be produced, then removed and put through the calender again for each additional pass. In an industrial process, more than five passes may be possible because the process would be continuous with multiple sets of rollers to ensure constant tension and alignment throughout.

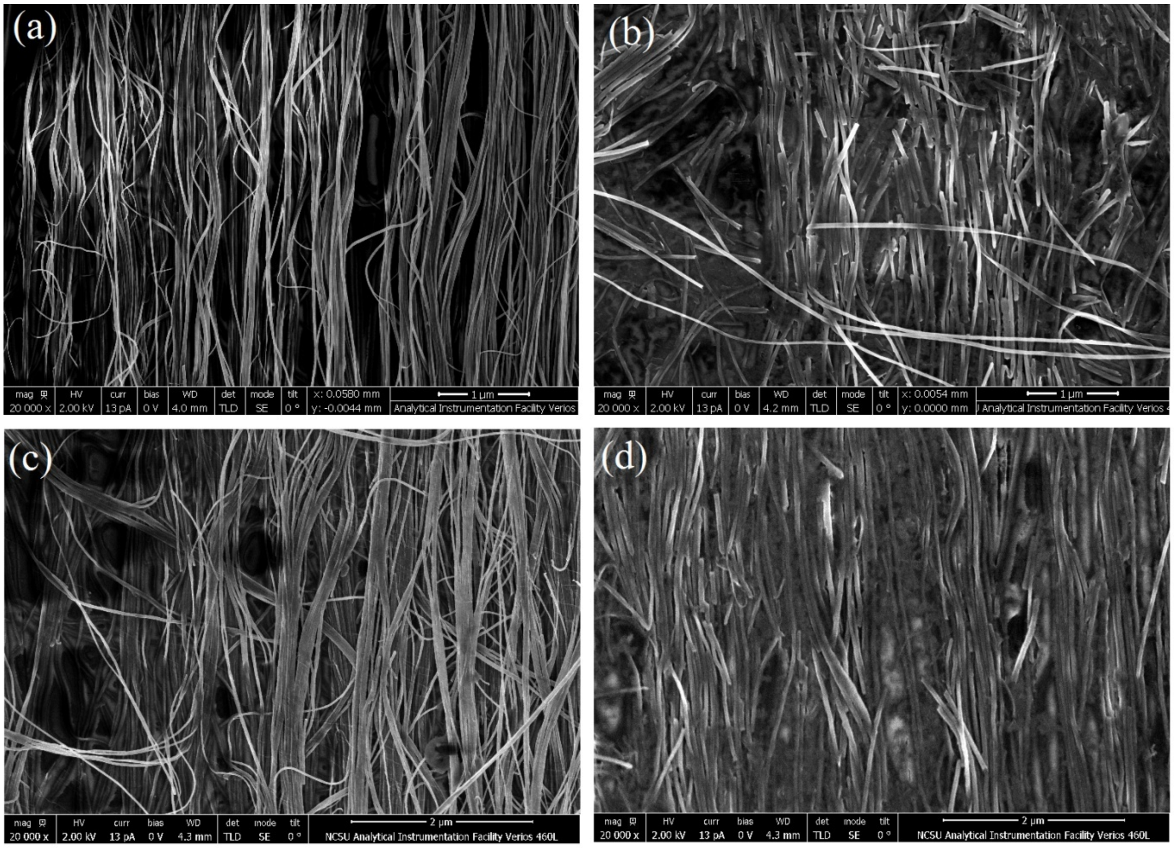

Figure 5.2 SEM images of (a) 1 pass unwiped, (b) 1 pass ethanol wiped, (c) 5 pass unwiped, and (d) 5 pass ethanol wiped samples

Atomic force microscopy was performed on the one, three and five pass samples to observe the surface characteristics imparted by the CNTs. Only the ethanol wiped samples could be tested via AFM because the presence of loose and unembedded CNTs caused the probe tip to snag and resulted in distorted images with inconsistent surface profiles. For each sample, a 100 μm^2 area was tested and 512 measurements were taken. Figure 5.3 shows the average surface roughness of each sample. The zero pass sample is the control sample and is simply the plain PETG film as it was received with no CNTs or post processing performed. From the data, we can see the average surface roughness increased as the number of passes increased. With the plain film only having a surface roughness of 0.224 nm, the presence of the CNTs caused a significant increase in surface roughness. The surface roughness increased from 28.807 nm (one pass) to 54.651 nm (five passes) with the three pass sample falling in between at 37.413 nm. This trend indicates there are more CNTs embedded in the film with increasing passes through the calender. The embedding of the CNTs alters the surface characteristics of the film, as shown in Figure 5.3b. With a higher amount of embedding, the surface of the film should become rougher due to more CNTs being present. After only one pass, more of the CNTs from the sheet were able to be removed by wiping and thus there was more undisturbed PETG film with smoother surface characteristics. Increasing the number of passes through the calender caused more complete and partial embedding of the CNTs which resulted in less being able to be removed from the surface by wiping. It should be noted that although the trend in surface roughness is indicative of better embedding, the average values may not be indicative of that of the entire sample. The CNT sheet is non-uniform and the surface characteristics of the produced film may vary over a large area.

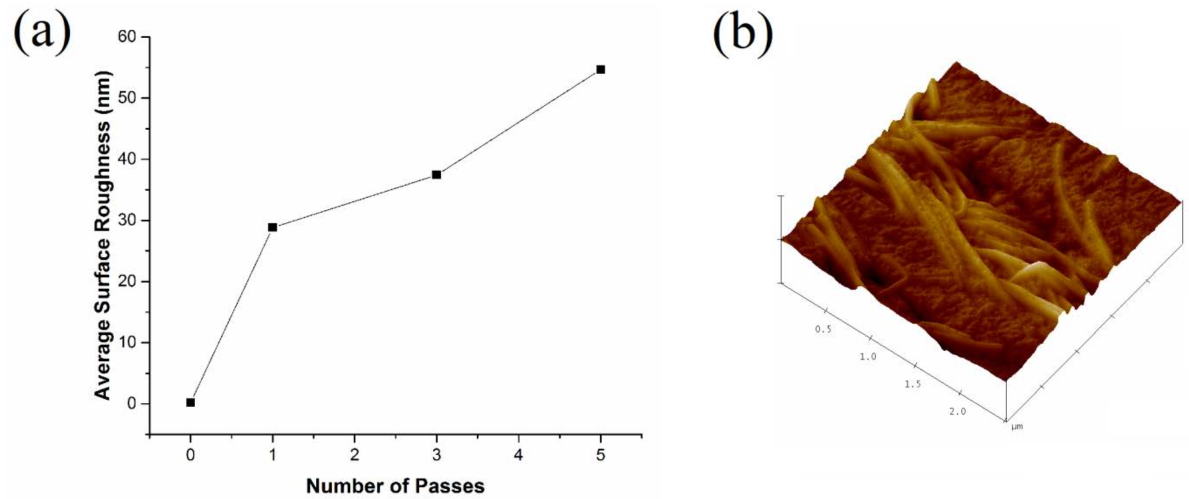

Figure 5.3 (a) Atomic force microscopy analysis of the surface roughness of samples produced with various passes through the calender and (b) a 3D rendering of a sample analyzed with AFM.

5.2 Variable Growth of Carbon Nanotubes

After optimizing the process and analyzing the electrical and optical trends of samples made from the same CNT array, the next step was to alter the CNT array parameters and determine how the morphology of the CNTs affect the optoelectronic properties. The most direct way to alter the CNT parameters is to perform the growth for a different amounts of time which will yield arrays of varying heights. In addition to the standard 20 minute growth time, CNT arrays were also grown for 5 and 10 minutes. Samples with growth times of less than 5 minutes were also made, however the spinnability was not adequate. A possible explanation for this is that in the early stages of growth, the CNTs grow in a wavy morphology and are not very aligned, which does not allow for the Van der Waals forces necessary for the CNTs to attach as they are pulled out synchronously. After growth the heights of the CNT arrays were analyzed using an optical microscope. Table 5.2 displays the growth times and the corresponding approximate heights of the arrays. Referring back to section 3.1.1, it is important to note that the CVD gas setup was altered during the variable growth experiments. Initially, the same setup in the previous experiments was used. A common problem during these experiments was inconsistent spinnability of CNTs grown for times shorter than 20 minutes. By utilizing residual gas analysis, it was determined that the argon/chlorine mixture was inconsistent and the concentrations would vary during and between growth runs. To resolve this problem, a pure chlorine tank was installed in place of the argon/chlorine mixture. This ensured a constant chlorine concentration and improved the uniformity of spinnability across the array. The results in this section were obtained using CNTs grown with the pure chlorine gas. To view the results obtained from the variable growth trials with the previous setup, see Appendix A.

Table 5.2 Growth times of vertically aligned spinnable CNT arrays grown via CVD and corresponding heights.

Growth Time (min)	Height (mm)
5	0.5
10	1.0
20	1.6

The diameters were also measuring using TEM images. Measurements were taken of 100 different individual CNTs from each array and averaged to achieve a representative result. The results can be seen in Figure 5.4. From these measurements, it can be seen that the average diameter of the CNTs increased with increased growth time. While there is a broad range of diameters for each growth time, the histograms exhibit a general shift to the right with increasing growth time. To determine if these results were significantly different, an analysis of variance (ANOVA) test was used. ANOVA was deemed appropriate because the samples are independent, the variances are similar, and by the central limit theorem, the samples are normally distributed. The null hypothesis for this test, H_0, stated that all means were equal, while the alternative hypothesis, H_a, stated that not all means were equal. Using an F-table corresponding to $df_1 = 2$ and $df_2 = 297$ at $\alpha = 0.05$, the rejection region is $F > 3.03$. Because the computed F statistic was 46.95, the null hypothesis was rejected and it was concluded that the growth time made a significant difference in the resulting tube diameters. While there are many factors involved, a possible explanation for the increase in diameter with increasing growth time was proposed by Hasegawa and Noda [101]. As the growth duration increases, the catalyst particles coarsen. This coarsening can be explained by Ostwald ripening, where larger catalyst particles increase in size while smaller particles decrease in size due to their higher strain energy and ultimately disappear due to atomic interdiffusion [102]. Over time, the total number of particles decreases and the average diameter increases which causes a lower overall density. Another cause for the increased diameter, as shown by Faraji et al. [103], is that the acetylene used during the growth process can deposit carbon on the tube walls which grows the CNTs radially.

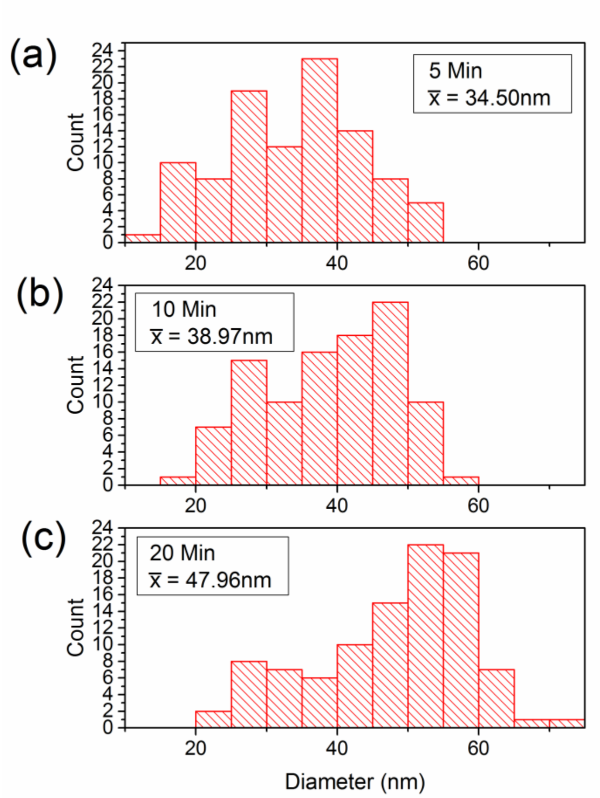

Figure 5.4 Histograms of the diameter measurements of CNTs grown for (a) 5 minutes, (b) 10 minutes, and (c) 20 minutes.

Table 5.3 ANOVA results of variation of CNT diameters from variable growth times.

Source	SS	df	MS	F Statistic for $\alpha = 0.05$
Between Samples	9396.1	2	4698	46.95
Within Samples	29718.4	297	100	
Total	39114.5	299		

Both the CNT diameter (influenced by the number of walls) and height have been shown to play a role in the electrical and optical properties. Longer CNTs with larger diameters will have a greater tendency to agglomerate and form bundles due to increased contact area between the CNTS. The presence of bundles has a significant effect on the transparency of the CNT films. Figure 5.5 shows images taken of samples produced with 5, 10, and 20 minute grown CNTs using an optical microscope. From these images, the increased bundling can be seen with increasing growth time. Chen et al. studied the effect of wall number and diameter on the electrical properties of CNT thin films and determined that there were offsetting factors that occurred with increasing the wall number (and thus, increasing diameter) [104]. While the height remained constant, increasing the wall number resulted in increased effective electrical conductivity however the packing density decreased. The effective electric conductivity increases because the metallicity of the CNTs increases with increasing wall number [105]. Because conduction occurs through the outermost shell, increasing the diameter causes the energy gap to decrease. This increased electrical conductivity is offset by the decrease in packing density that comes with a higher number of walls. Having fewer CNTs per unit area reduces the number of contact points and increases the chances of gaps that will increase resistance. The study by Chen et al. as well as a study by Li et al. [106] concluded that CNTs with approximately 2 walls (DWCNTs) exhibit a superior combination of electrical and optical properties compared to SWCNTs and MWCNTs. Unfortunately, the growth setup used in this process is unable to produce DWCNTs at this time. The size of the catalyst that precipitates out of the vapor phase is the main factor in determining CNT size and this depends on the total chamber pressure, the partial pressures of the catalyst vapor and gases, and the temperature. It may be possible to alter these conditions and still achieve spinnable arrays, but because there is such a small window for array spinnability in terms of alignment, catalyst spacing, and density, altering the established growth setup was not explored. However, this could be an interesting avenue for further research.

Figure 5.5 Presence of CNT bundling shown in samples produced with CNT arrays grown for (a) 5 minutes, (b) 10 minutes, and (c) 20 minutes.

After growing and analyzing the dimensional attributes of the CNTs, films were produced using the same method discussed in the previous section. Based on the findings from the previous section, the measurements were taken on samples passed through the calender one time and five times. Figure 5.6 shows the electrical and optical measurement results of these samples. Only unwiped and ethanol wiped samples were tested. Dry wiping was not performed because based on the previous results, there is little difference between the unwiped and dry wiped samples under these processing conditions. From these results, it can be seen that the resistance and transmittance decreased as the growth time increased. These results were expected because, as previously discussed, the height and diameter of the CNTs increases with increasing growth time. The CNTs with a larger diameter will absorb more photons and the corresponding height increase results in more bundling because there is more contact between the CNTs. The bundles are agglomerations of CNTs that will absorb more photons than an area of well aligned and evenly spaced CNTs. The increased number of walls and diameter increases the metallicity of the CNTs which decreases the resistance. Furthermore, the increased height allows for more contact points between the CNTs which decreases the chances of an open gap of insulating polymer existing within the measured area which would increase the resistance. The tradeoff between transparency and sheet resistance can be seen with these samples. For the one pass unwiped samples, the 5 minute grown array (height = 0.5mm, average diameter = 34.5nm) had an average sheet resistance of 1921 Ω/square at an average transmittance of 65.83%. Both values decreased for the 10 minute grown sample (height = 1.0mm, average diameter = 38.97mm) to 1623 Ω/square and 55.94%. A more drastic decrease was seen when using the 20 minute grown sample (height = 1.6mm, average diameter = 47.96nm) to 384 Ω/square and 43.56%. The gap in sheet resistance between each individual wiped and unwiped sample decreased as the growth time increased. A possible explanation is that when using taller CNTs during the process, more out of plane tubes are likely to become at least partially embedded and unable to be removed by wiping. Shorter CNTs have less length that can become partially embedded in the film and thus may have more unembedded CNTs that can be removed from the surface by wiping. Furthermore, the gap in transmittance between the unwiped and wiped CNTs increased with increasing growth time. This can be explained through bundling. Taller CNTs with more walls are more likely to form bundles during processing [26]. Bundles provide more contact points for electrons to travel but also absorb more photons because of a high density of CNTs. Because the bundles are thicker and are likely to contain many out of plane CNTs, the level of embedding is expected to be relatively low compared to the non-bundles areas. By wiping with ethanol, the unembedded CNTs within the bundles will be removed and the transparency of the film will increase. Shorter CNTs are less likely to form bundles and thus there is less room for increasing transparency under the same processing conditions. Table 5.4 shows the differences between samples with different growth times at the wiped and unwiped stages. From these images, it can be seen that the haziness of the unwiped increases with increasing growth time which is indicative of CNT bundles in the film.

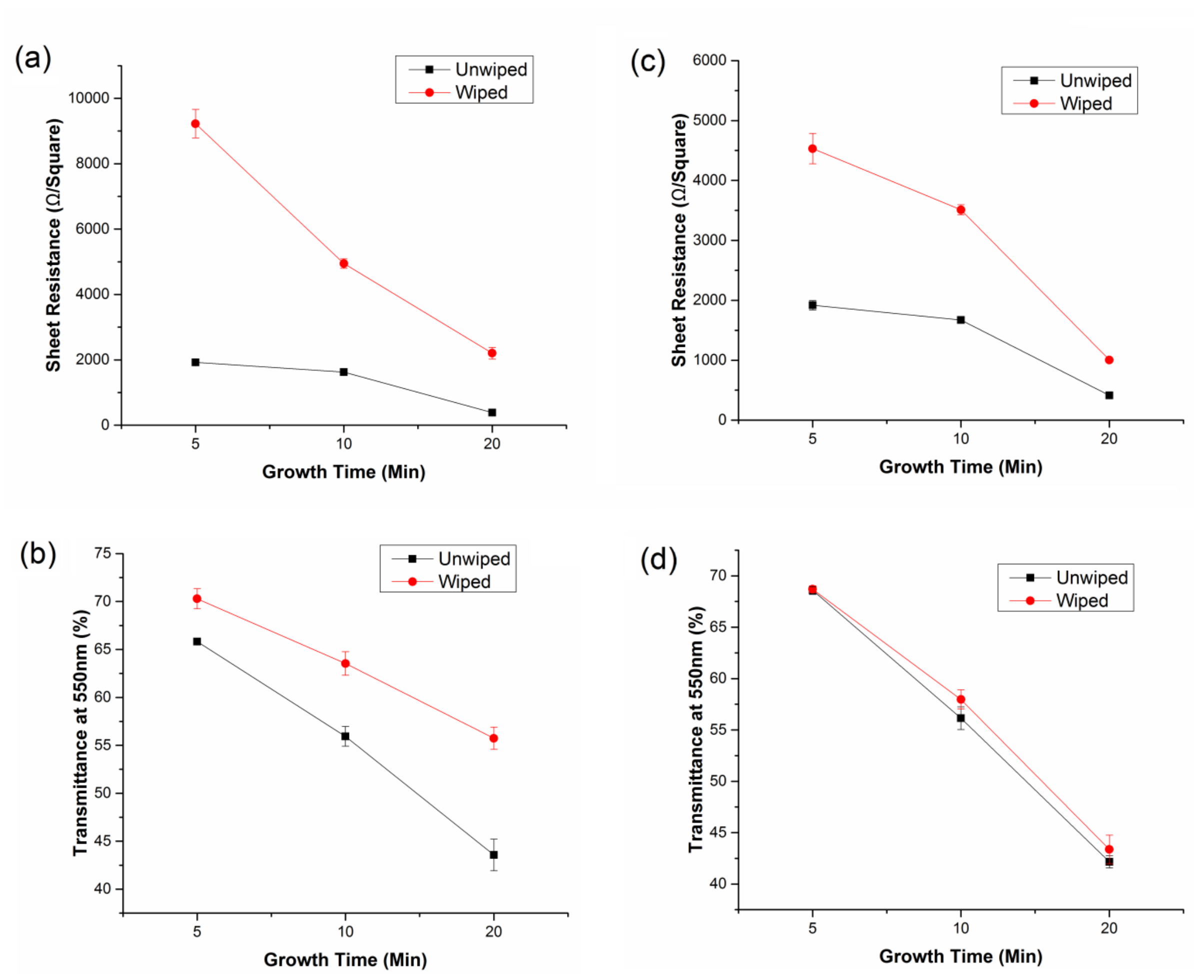

Figure 5.6 Sheet resistance vs. growth time and transmittance vs. growth time for (a) and (b): 1 pass samples and (c) and (d): 5 pass samples.

Table 5.4 Visuals of samples produced with variable growth times showing the progression of transmittance upon wiping

Growth Time	5 Min	10 Min	20 Min
Unwiped		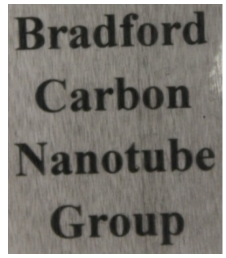	
Wiped	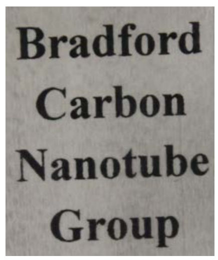	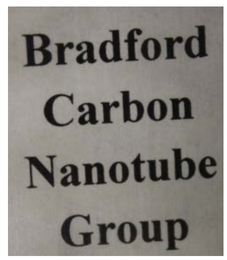	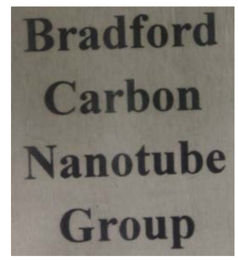

In addition to height and diameter, another aspect of the CNTs that affects the electrical properties is the defect density. To analyze this, Raman spectroscopy was used. It is necessary to analyze the D-band (1350 cm^{-1}) and the G-band (1582 cm^{-1}). The D-band is indicative of any disorder in the material that may lower the crystal symmetry of the lattice and the G-band is induced by in-plane vibration of graphite within the material [107]. By comparing ratio of the G-band and D-band intensity peaks (G_I/D_I), the relative defect density and graphitic quality can be ascertained [108]. For this experiment, each array was analyzed using Raman spectroscopy. The laser was focused on at the front of each array lengthwise and at the middle widthwise to attain values that best relate to the electrical and optical measurements. In addition to determining the difference between each array, it is relevant to analyze the variation within an array. Because the process is continuous, it is important to know if the quality and defect concentration vary along the length of the array. In order to determine the variation in quality and defects along the array, the 10 minute array was chosen and Raman measurements were taken at the front, the middle, between the middle and back, and at the back of the array. Furthermore, the consistency of our growth process was assessed. Three different arrays were grown for 10 minutes each under the same settings and each array was analyzed. These results can be seen in Figure 5.7 As seen in 5.7a, G_I/D_I increased with increased growth time. This indicates a decrease in defect concentration with increasing growth time. The decrease in defect concentration contributes, along with the diameter and height, to the decreasing sheet resistance with increasing growth time. From Figure 5.7b, it can be seen that G_I/D_I remained constant from the front to the middle of the array but decreased in moving from the middle to the back. A common problem with the arrays is the decrease in spinnability at the back of the array. This data indicates that the defect density increases, which is a contributing factor to this problem. Figure 5.7c shows that there is variation in defect density between arrays grown in our reactor. Two of the arrays showed the same G_I/D_I of 1.60, however the third array increased to 1.72. The controllable settings (catalyst amount, gas flow, temperature, pressure, growth time, post treatment time, and position within the furnace) remained constant, however factors such as catalyst quality, moisture content, and flow dynamics within the reactor may contribute to this variation. With further research and monitoring accessories within the reactor, it should be possible to improve the consistency between arrays.

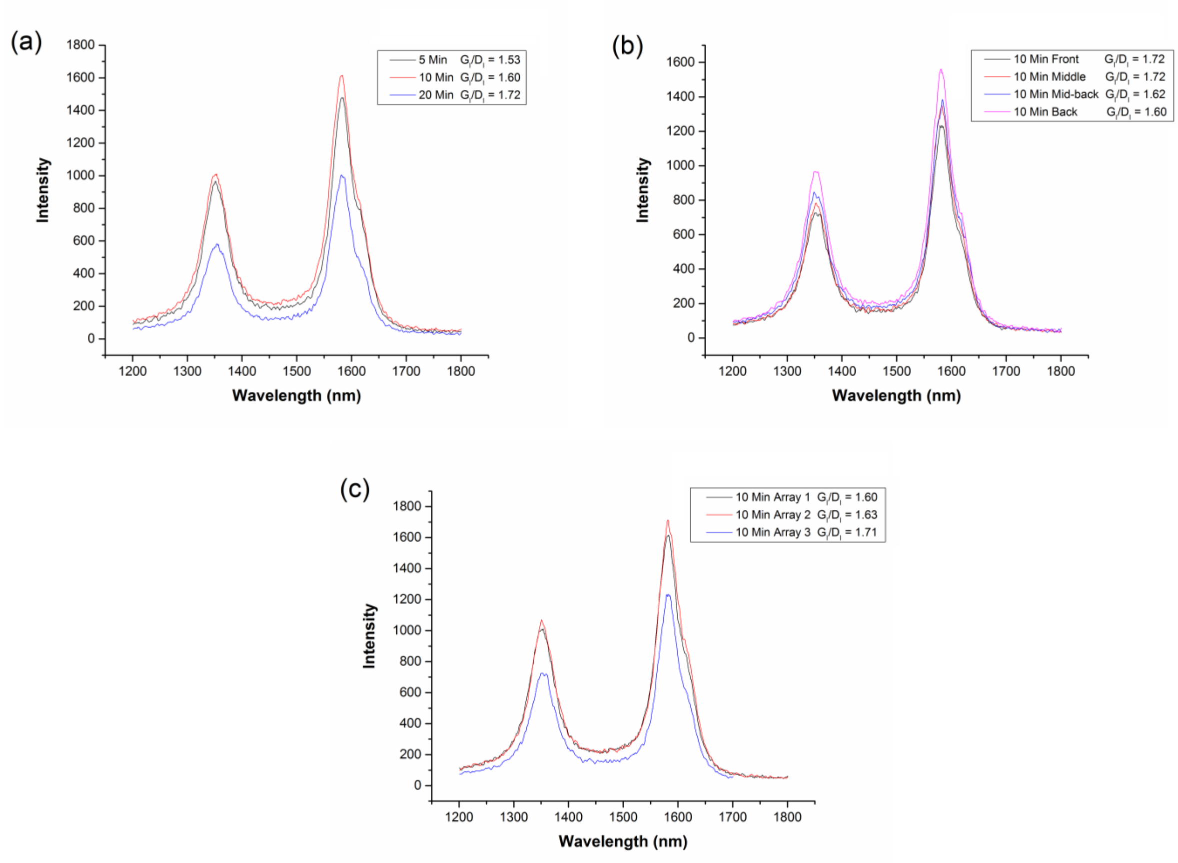

Figure 5.7 Raman spectroscopy analysis of (a) 5, 10 and 20 minute grown arrays, (b) variation along length of a single 10 minute grown array, and (c) variation between different arrays grown under the same conditions.

To further confirm the effect of G_I/D_I on the electrical properties of the produced film, samples were produced using the positions and arrays from Figure 5.6b and 5.6c. Only one pass unwiped samples were analyzed because the basic properties of the CNT sheet were the main focus. Adding additional passes and wiping may introduce more variation between the samples which is undesirable for these basic comparisons. Figure 5.8 shows the results from these trials. As expected, the sheet resistance decreased as G_I/D_I increased. Although other factors may influence the sheet resistance as well, it is reasonable to conclude that the defect concentration is a key contributor to the variation in sheet resistance within and between the arrays. Improving the consistency of electrical properties within and between arrays should be further studied in order to achieve appropriate properties for applications with tight tolerances.

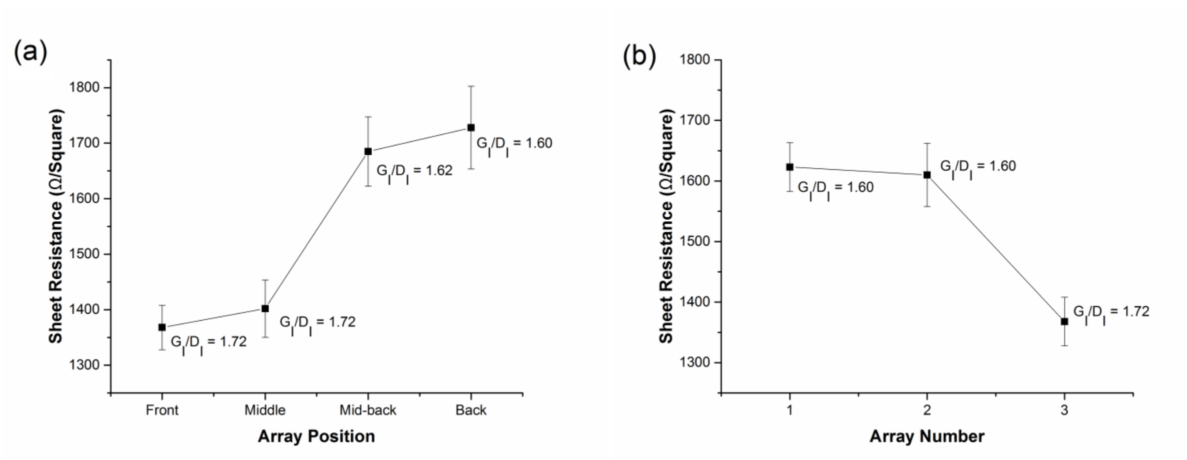

Figure 5.8 Sheet resistance measurements showing variation of (a) positions along one array and (b) between different arrays.

To analyze the change in mechanical properties of the film due to embedding CNTs in the surface, nanoindentation was used. The methods and set up used are described in Section 3.5.4. During testing, the surface of the film is indented and the resistance to indentation is monitored. From this data, the Young's modulus and hardness of the material can be determined. These tests were performed on the one pass and five pass ethanol wiped samples using the 5, 10, and 20 minute grown arrays. The unwiped samples proved problematic and gave inconsistent results which was due to unembedded CNTs on the surface shifting during indentation. The modulus and hardness are both a function of the indentation load. For comparison purposes, only the data from a 50μN load is displayed in Figure 5.9. It should be noted that the modulus and hardness values will decrease with increasing load.

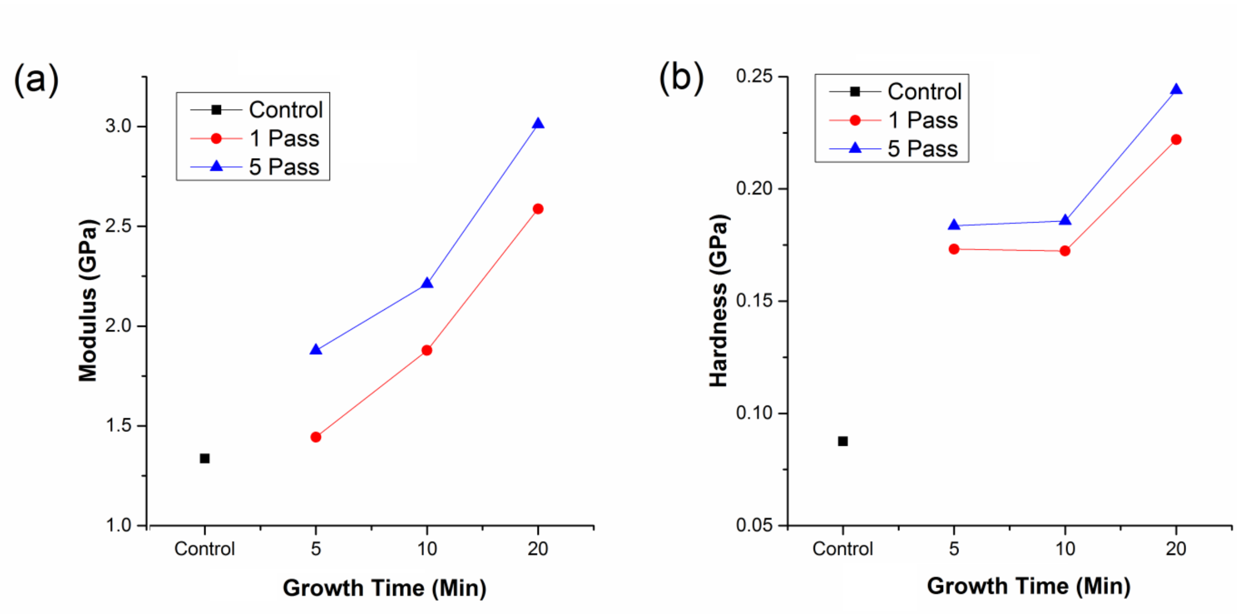

Figure 5.9 (a) Young's modulus and (b) hardness values calculated from nanoindentation data for wiped samples produced with 5, 10, and 20 minute growth arrays at a load of 50 μN.

The nanoindentation results show that both the modulus and hardness increase when using CNTs grown for longer periods of time. As expected the modulus and hardness both increase from one to five passes through the calendar. This is a result of there being more CNTs embedded in the surface of the PETG film after five passes compared to only one pass. The nanoindenter can calculate the reduced modulus, E_r, based on the slope of the load-displacement curve. From the reduced modulus, the Young's modulus can be calculated from the following equation:

$$\frac{1}{E_r} = \frac{(1 - \nu^2)}{E} + \frac{(1 - \nu_i{}^2)}{E_i}$$

Where ν_i and E_i are the poisson's ratio and Young's modulus of the indenter material, in this case diamond. These values are 0.07 and 1140 GPa, respectively. ν and E are the poisson's ratio and Young's modulus of the material being measured. In the case of these films, the poisson's ratio was estimated at 0.35. It is likely that the hardness and Young's modulus can both be attributed to the diameter and number of walls of the CNTs. With more walls, the CNTs should become stiffer in the transverse direction and more resistant to indentation. By increasing the number of passes and thus the number of CNTs embedded in the surface of the film, the nanoindenter is less likely to contact bare polymer which gives an overall increase in hardness and modulus across the measured areas. These improved mechanical properties may be beneficial to some applications where the surface may be vulnerable to scratching or impact.

5.3 Additional Improvements and Applications

5.3.1 Effect of Acid Treatment on Electrical Properties

Various studies have shown that treating CNTs with acids can improve the electrical properties. Kaskela et al. [109] demonstrated this increase in electrical properties by treating CNT transparent films with nitric acid. It was shown that this treatment caused p-type doping of the CNTs with electron acceptors which increased the conductivity of the semiconducting

CNTs. Because the majority of transparent CNT conducting films in literature are produced via dispersion, there has been debate over whether the main benefit of the acid treatment is doping or simply removal of the solvent or dispersion fluid from the CNTs. Shin et al. [110] conducted experiments and showed that the p-type doping has a larger effect on the sheet resistance than the removal of residual dispersant. These results show that the acid treatment could be beneficial for the samples produced in this study because the CNTs are directly incorporated into the polymer film with no dispersion necessary. A study by Geng et al. [111] determined that the ideal treatment time in nitric acid for CNT transparent films was one hour. After one hour, the sheet resistance began to increase due to the CNTs being damaged.

For the following experiments, the samples were treated in 50% HNO_3 for one hour. To initially determine how the acid treatment affected the samples at various stages of calender passes and wiping, only the samples produced using the 20 minute grown array were used. The results can be seen in Figure 5.10. From these results, it can be seen that the sheet resistance decreases by 33% (384 to 257 Ω/square) for the one pass unwiped sample, however there is little to no decrease in sheet resistance for the other samples. Because the wiped samples as well as the five pass sample have fewer CNTs on the surface, the HNO_3 is unable to contact and dope as many CNTs as with the one pass unwiped sample. Because of this, there is little to no effect seen in regards to the sheet resistance. An added benefit of the HNO_3 treatment, as shown in Figure 5.10b, is that there is little change in the transmittance. Based on these results, the HNO_3 treatment is beneficial for the 1 pass unwiped samples that have many CNTs exposed on the surface of the film, however it is not beneficial for the wiped and 5 pass samples that have fewer CNTs exposed.

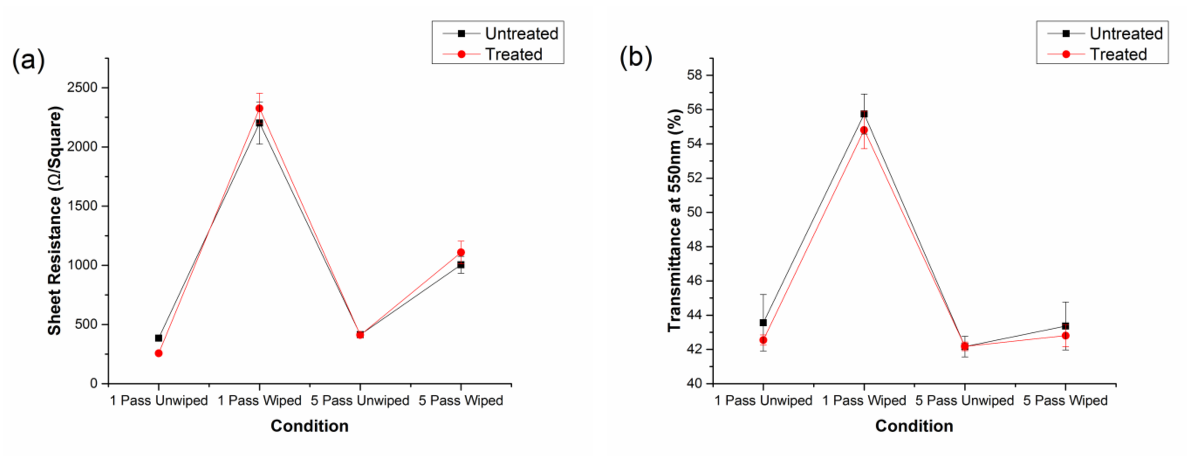

Figure 5.10 Comparison of (a) sheet resistance and (b) transmission for untreated and HNO3 treated samples at various stages.

After analyzing the previous results, the samples produced with the 5 and 10 minute grown arrays were treated as well to determine if the effect of the treatment differs based on the CNT parameters. As shown in Figure 5.11, a similar trend follows for the samples produced with 5 and 10 minute grown arrays. The 10 minute sample exhibited a 37.6% decrease (1623 to 1012 Ω/square) and the 5 minute sample decreased by 16.8% (1921 to 1596 Ω/square). Similar to the previous results, the transmission data showed little change after the acid treatment. These results show a promising method to improve the electrical properties of the CNT films without significantly affecting the optical properties. Further research of this treatment in regards to acid type, concentration, and duration will be helpful in fully optimizing the properties of the films.

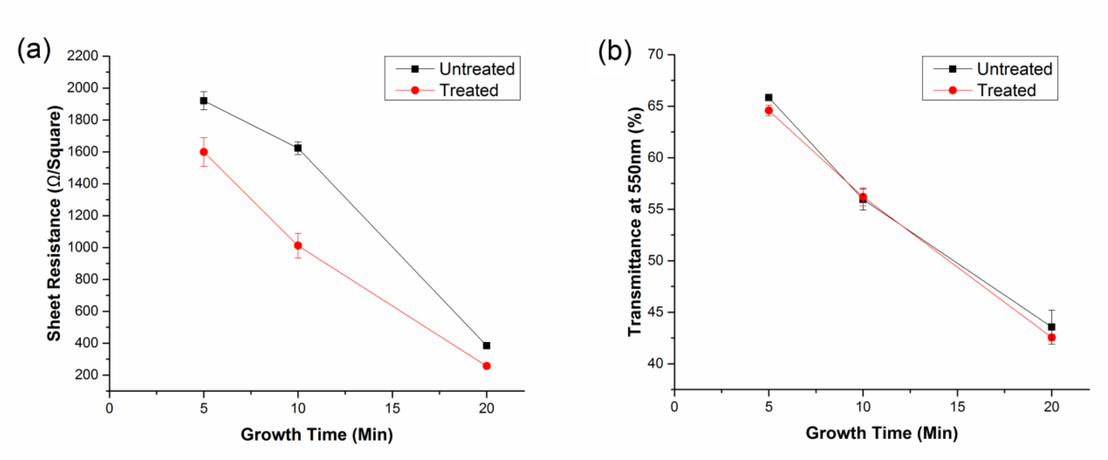

Figure 5.11 Comparison of (a) sheet resistance and (b) transmission for untreated and HNO3 treated samples using CNT arrays grown for 5, 10, and 20 minutes.

5.3.2 Bending Tests

A key benefit of using CNTs to make semi-transparent conductive films is the flexibility. Although ITO can be deposited on flexible polymer films, the electrical properties decline upon flexing. Very short CNTs (10 µm) may rupture upon bending, which was the case in [28]. However our CNTs are much longer and are able to remain intact and bridge across the elongation induced by bending. To exhibit the effect of bending on the electrical properties of the samples produced in this research, a simple screw driven adjustable plate was used. Two 12mm x 50mm piece of film were cut from a one pass unwiped sample produced from a 20 minute grown array, one with the CNTs parallel to the ends and one with the CNTs perpendicular. The lead wires were attached at each end using silver epoxy and were connected to a multimeter which displayed the resistance. The screw was then turned to decrease the distance between the plate and the edge and the bend radius was measured using a ruler. Figure 5.12 shows the experimental set up and Figure 5.13 shows the resulting data after bending. After the minimum bend radius was achieved, the film was then completely folded over.

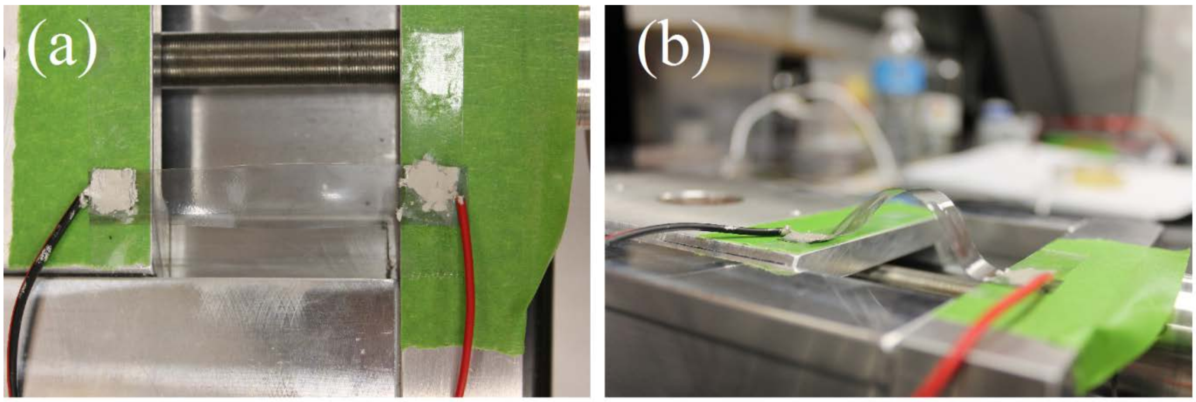

Figure 5.12 Bending test set up showing the leads connected to each end of a (a) flat sample and (b) bent sample.

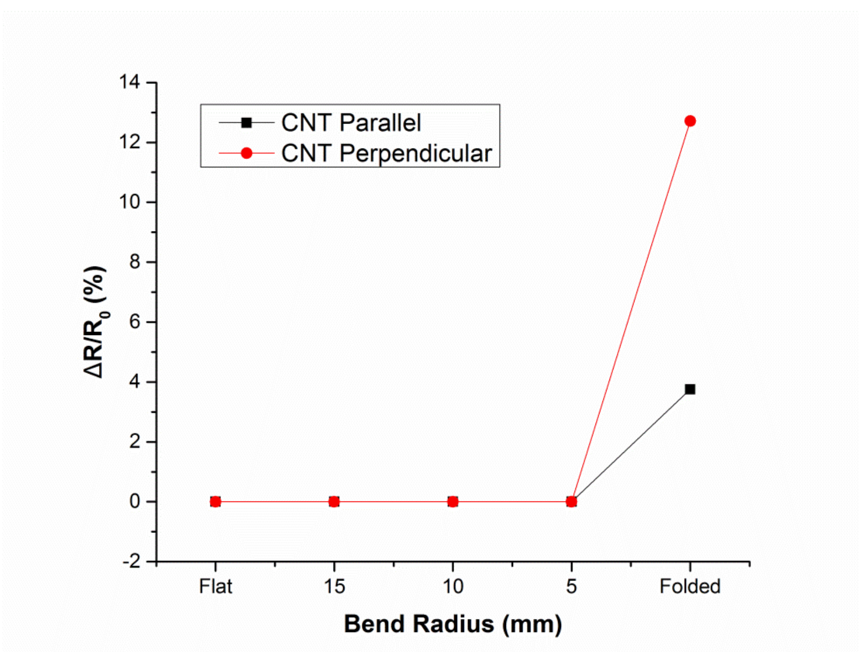

Figure 5.13 Resistance change as a function of bend radius for samples with the CNTs parallel and perpendicular to the bend direction.

These results show that there was virtually no change in resistance upon bending and only a 4% increase for the parallel direction and a 13% increase for the perpendicular direction when the sample was folded. These results are superior to the results obtained by Feng et al. [81] using a CNT-PET film produced from a spinnable CNT array. In this study, the resistance remains constant during bending but increases by 13% upon folding, two orders of magnitude higher than our results. An ITO-PET film was also measured by Feng et al. and it was found that the resistance increased by 30% at a bending radius of 5mm and by 12708% upon completely folding which indicates that bending causes the ITO to crack. Although the optical properties are not up to par with ITO, the combination of flexibility while maintaining fairly constant resistance of these CNT films provides a unique attribute that may be useful in some applications that require extreme bending of the film.

5.3.3 Piezoresistive Strain Sensing

One potential application of these semi-transparent CNT conductive films is as a strain sensor. CNTs exhibit piezoelectric behavior which causes the electrical resistance to change as strain is applied. By monitoring the change in resistance of the conductive CNT films upon straining, a model can be developed and unknown strains can be determined based on the change in resistance of the film. The strain sensing capabilities of CNT-polymer films have been exhibited [112-114], however in most cases the films are fabricated using a dispersion method. The calendering process utilized in this research would be beneficial in quickly producing films that could be cut or directly applied as strain gauges with few no to extra steps necessary.

To test the strain sensing performance of CNT films produced in this research, monotonic tensile tests were performed as described in Section 3.5.4. Samples were tested with the CNT alignment parallel and perpendicular to the loading direction. The results can be seen in Figure 5.14. From these results, it is apparent that the CNT orientation significantly affects the piezoresistive behavior of the films. With the CNTs parallel to the loading direction, the response was much more sensitive than with the CNTs perpendicular. The main mechanisms that can explain the piezoresistive behavior of the CNT films involve the CNT interconnections and the tunneling effect between individual CNTs [115]. Under normal conditions, the CNTs in the film have many contact points with one another due to the general alignment and the presence of bundles. As the film is strained, the CNTs will shift and possibly break. This movement can create more junctions where CNTs are not connected and there is a gap between them.

The high sensitivity of the parallel sample can be attributed to the previously discussed factors. Because the strain is being applied in the same direction of the CNT alignment, the movement will likely shift the CNTs and decrease the number of contact points which are the primary mechanism of electrical conductivity in this direction. Decreasing the number of contact points causes a more difficult path for electrons to travel which increases the resistance reading. The strain may also cause tearing or cracking along the CNT direction which would further contribute to this increased resistance. Another factor that may play a role is load transfer to the CNTs. CNTs have intrinsic piezoelectric properties and straining of the individual CNTs in the film should allow this to contribute to the overall resistance change. Although a complete analysis was not performed, one potential reason the sample with the CNT film perpendicular to the loading direction showed very low sensitivity is that tunneling could be the main mechanism for resistance within the sample. Although there are some crossover points because the CNTs are not perfectly aligned, the resistance is generally governed by tunneling where electrons must travel across the insulating polymer between the CNTs in the perpendicular direction. By increasing the strain, the gaps could slightly increase, however this should not significantly affect the overall resistance. Any damage or cracks that occur in the film will be in the transverse direction to the CNTs and thus will not significantly affect the resistance that is controlled mainly by tunneling. As shown by the parallel sample, contact points between the CNTs are a much more influential aspect of overall resistance.

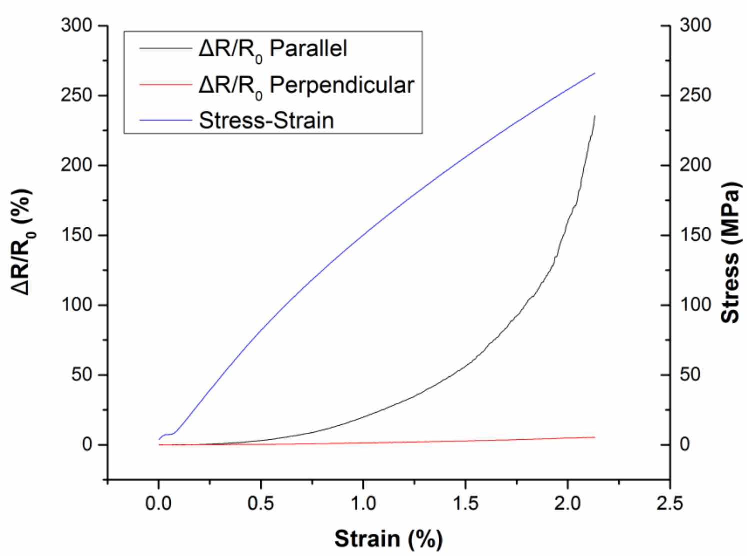

Figure 5.14 Piezoresistive behavior of the CNT films during monotonic tensile testing.

These promising results show that the films produced in this research could potentially have applications as strain sensors where transparency is necessary. The films are simple to apply to a desired substrate and may be cut to various sizes to fit. Utilizing the films with the CNTs aligned parallel to the loading direction is much more beneficial than having them aligned in the perpendicular direction in terms of sensitivity. The elastic nature of the PETG film should also allow for strain sensing at higher strains that those demonstrated in this research. Further research will be necessary to determine the correlation between the sensing capabilities and the transparency of the films.

5.3.4 Electrically Induced Heating

Another potential application for these CNT films is for use as a semi-transparent film heater for use as defrosters. ITO coated substrates are often used as transparent heaters, however limitations arise from slow thermal responses, inflexibility, and intricate production methods. CNTs could provide a new material with additional benefits as transparent film heaters due to their electrical and thermal conductivities. CNT film heaters have been produced using both dispersed CNTs [116] and CNTs drawn from aligned arrays [117, 118]. Using aligned CNTs is beneficial for potential mass production of the heaters because there are fewer steps involved in fabrication.

For this experiment, the one pass unwiped samples produced with 5, 10 and 20 minute grown arrays were used to determine how the CNT parameters affect the voltage-temperature relationship. The testing setup can be seen in section 3.5.1. All samples were cut to the same size (1" x 2") and the same voltages and currents were used to ensure that there is no variation between samples in terms of input power and surface area. The thermocouple was placed directly on the film to achieve an accurate measurement of the surface temperature. Indirect temperature measurement may be affected by convection. Figure 5.15 shows the resulting temperatures as various voltages were applied to each sample.

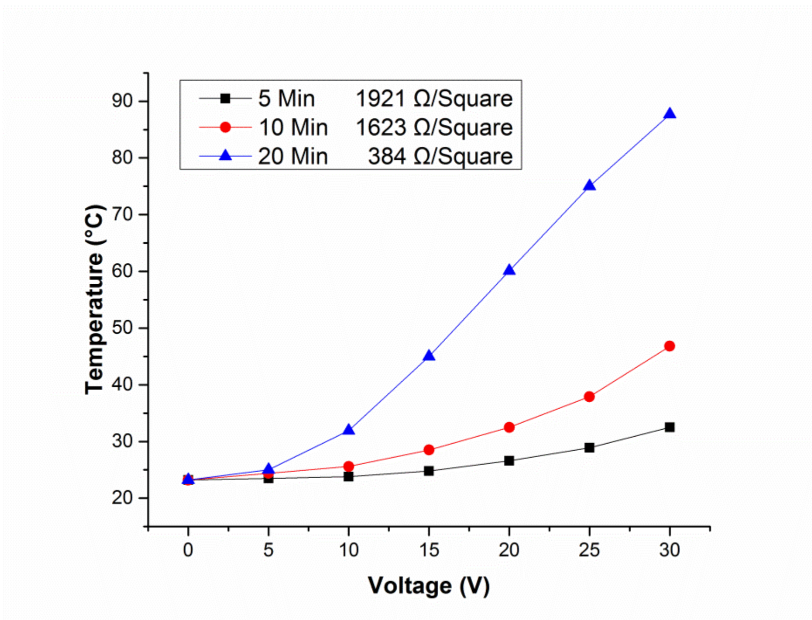

Figure 5.15 Temperature vs. voltage for 1 pass unwiped samples produced with 5, 10, and 20 minute grown arrays.

From this data, it can be seen that the 20 minute grown sample heats up much higher than the other two samples. At an applied 30V, the 20 minute sample reached a temperature of 87.7°C which was above the glass transition temperature of the PETG film and caused it to soften. The influence of sheet resistance of the films is very apparent from this data. Of course, the transparency decreases as sheet resistance decreases and high transparency is ideal for thin film heaters for use as defrosters. At a standard voltage of 12V, the 5 and 10 minute samples may not have adequate electrical properties and the 20 minute sample may not meet transparency standards. Further research could be done with these films in order to optimize the resistance and transparency of the films for use as thin film heaters. These preliminary results show that the films produced in this research do exhibit electrically induced heating and may be adequate for applications with further optimization. The flexibility of the films and the simple fabrication through a continuous process make them an intriguing material for future research.

5.4 Conclusions

The results from this section show that by altering the growth times of the CNTs, their height and diameter can be altered. These properties influence the electrical and optical properties of the CNTs. This influence was shown by embedding the CNT sheets from different arrays using the same calendering process and measuring resulting the properties of the conductive films. Performing a post production nitric acid treatment was shown to lower the sheet resistance of the films via p-type doping without affecting the transparency. The lowest sheet resistance (257 Ω/square) was obtained after acid treating a sample passed through the calender only once at 135°C without wiping. This sample had a transparency of 42.55%. The highest transparency achieved (70.29%) corresponded to a 5 minute grown sample that was passed through the calender once at 135°C at wiped with an ethanol soaked cloth afterwards. The sheet resistance of this sample was 9224 Ω/square. The relationship between sheet resistance an transparency is exhibited throughout this study. Applications such as strain sensing and electrical film heaters were demonstrated, although further research is required to optimize the properties and determine the viability for consumer industry. More research must go into improving the properties and consistency of the CNTs, however the flexural properties of the produced films and simple continuous fabrication process make these films unique with the potential for scaling up to industrial production.

6 Suggestions for Future Work

Although this research has presented a viable process to directly incorporate CNTs into a polymer film through a continuous process, there is much room for further research. In regards to the calendering process, more polymers and roller coverings should be tested A better non-stick relationship between another cover and polymer film may be found that allows for more compression of the film that was unattainable with the Teflon and PETG film due to deformation. With the ability to compress the film more, it may be possible to better embed the CNTs without the need for additional passes. Being able to obtain optimal properties with only one pass through the calender would be more appealing for industrial production due to decreased production time which would allow for higher throughput. A polymer with a lower glass transition temperature would also require less heating and thus lower energy consumption.

Additional research is also required in the area of vertically aligned spinnable CNTs. Although the processing parameters do affect the resulting film, the CNTs are the dominating factor in regards to the final optical and electrical properties. As demonstrated in this research, there is variability in the properties within and between CNT arrays grown under the same set of conditions. In order to meet tight tolerances that some products may require, the uniformity and consistency of the arrays will need to be improved. Because there are many factors involved, multiple studies will be required to analyze aspects such as temperature, pressure, catalyst, substrate, and precursor gases to determine their affect on spinnability, uniformity, and consistency of properties of arrays. Ideally very tall CNTs with few walls and good spinnability will be produced which will result in films with high transparency and low sheet resistance. Furthermore, methods by which to improve the electrical and optical properties of the spinnable CNT arrays after growth should be explored. Methods to reduce or eliminate bundles and dope the CNTs during processing would be beneficial in improving the optical and electrical properties. Incorporating these methods into the continuous process would add greater benefit.

REFERENCES

[1] Monthioux, M., & Kuznetsov, V. L. (2006). Who should be given the credit for the discovery of carbon nanotubes? *Carbon, 44*(9), 1621-1623.

[2] Iijima, S. (1991). Helical microtubules of graphitic carbon. *Nature, 354*(6348), 56-58.

[3] Ren, Z., Lan, Y., & Wang, Y. (2013). Aligned carbon nanotubes physics, concepts, fabrication and devices Springer Berlin Heidelberg.

[4] Dresselhaus, M. S., Dresselhaus, G., & Saito, R. (1995). Physics of carbon nanotubes. *Carbon, 33*(7), 883-891.

[5] Sears, A., & Batra, R. C. (2004). Macroscopic properties of carbon nanotubes from molecular-mechanics simulations. *Phys.Rev.B*, *69*(23), 235406.

[6] Rao, C. N. R., - Voggu, R., & - Govindaraj, A.- Selective generation of single-walled carbon nanotubes with metallic, semiconducting and other unique electronic properties - The Royal Society of Chemistry.

[7] Li, H. J., Lu, W. G., Li, J. J., Bai, X. D., & Gu, C. Z. (2005). Multichannel ballistic transport in multiwall carbon nanotubes. *Phys.Rev.Lett., 95*(8), 086601.

[8] Journet, C., Maser, W. K., Bernier, P., Loiseau, A., & et al. (1997). Large-scale production of single-walled carbon nanotubes by the electric-arc technique. *Nature, 388*(6644), 756-758.

[9] Scott, C. D., Arepalli, S., Nikolaev, P., & Smalley, R. E. (2001). Growth mechanisms for single-wall carbon nanotubes in a laser-ablation process. *Applied Physics A*, *72*(5), 573-580.

[10] Lee, C. J., Kim, D. W., Lee, T. J., Choi, Y. C., Park, Y. S., Lee, Y. H., . . . Kim, J. M. (1999). Synthesis of aligned carbon nanotubes using thermal chemical vapor deposition. *Chemical Physics Letters, 312*(5–6), 461-468.

[11] Baker, R. T. K. (1989). Catalytic growth of carbon filaments. *Carbon, 27*(3), 315-323.

[12] José-Yacamán, M., Miki-Yoshida, M., Rendón, L., & Santiesteban, J. G. (1993). Catalytic growth of carbon microtubules with fullerene structure. *Applied Physics Letters, 62*(6), 657-659.

[13] Robertson, J., Zhong, G., Esconjauregui, S., Zhang, C., Fouquet, M., & Hofmann, S. (2012). Chemical vapor deposition of carbon nanotube forests. *Physica Status Solidi (b), 249*(12), 2315-2322.

[14] Sinnott, S. B., Andrews, R., Qian, D., Rao, A. M., Mao, Z., Dickey, E. C., & Derbyshire, F. (1999). Model of carbon nanotube growth through chemical vapor deposition. *Chemical Physics Letters, 315*(1–2), 25-30.

[15] Hata, K., Don N. Futaba, Mizuno, K., Namai, T., Yumura, M., & Iijima, S. (2004). Water-assisted highly efficient synthesis of impurity-free single-walled carbon nanotubes. *Science, 306*(5700), 1362-1364.

[16] Li, W. Z., Xie, S. S., Qian, L. X., Chang, B. H., Zou, B. S., Zhou, W. Y., . . . Wang, G. (1996). Large-scale synthesis of aligned carbon nanotubes. *Science, 274*(5293), 1701-1703.

[17] Fan, S., Chapline, M. G., Franklin, N. R., Tombler, T. W., Cassell, A. M., & Dai, H. (1999). Self-oriented regular arrays of carbon nanotubes and their field emission properties. *Science, 283*(5401), 512-514.

[18] Sen, R., Govindaraj, A., & Rao, C. N. R. (1997). Carbon nanotubes by the metallocene route. *Chemical Physics Letters, 267*(3–4), 276-280.

[19] Grüneis, A., Rümmeli, M. H., Kramberger, C., Barreiro, A., Pichler, T., Pfeiffer, R., . . . Büchner, B. (2006). High quality double wall carbon nanotubes with a defined diameter distribution by chemical vapor deposition from alcohol. *Carbon, 44*(15), 3177-3182.

[20] Kumar, M., & Ando, Y. (2010). Chemical vapor deposition of carbon nanotubes: A review on growth mechanism and mass production. *Journal of Nanoscience and Nanotechnology, 10*(6), 3739-3758.

[21] Morjan, R. E., Nerushev, O. A., Sveningsson, M., Rohmund, F., Falk, L. K. L., & Campbell, E. E. B. (2004). Growth of carbon nanotubes from C60. *Applied Physics A, 78*(3), 253-261.

[22] Baker, R. T. K., & Waite, R. J. (1975). Formation of carbonaceous deposits from the platinum-iron catalyzed decomposition of acetylene. *Journal of Catalysis, 37*(1), 101-105.

[23] Baker, R. T. K., Barber, M. A., Harris, P. S., Feates, F. S., & Waite, R. J. (1972). Nucleation and growth of carbon deposits from the nickel catalyzed decomposition of acetylene. *Journal of Catalysis, 26*(1), 51-62.

[24] Jiang, K., Li, Q., & Fan, S. (2002). *Nanotechnology: Spinning continuous carbon nanotube yarns*

[25] Zhang, M., Atkinson, K. R., & Baughman, R. H. (2004). Multifunctional carbon nanotube yarns by downsizing an ancient technology. *Science, 306*(5700), 1358-1361.

[26] Liu, K., Sun, Y., Chen, L., Feng, C., Feng, X., Jiang, K., . . . Fan, S. (2008). Controlled growth of super-aligned carbon nanotube arrays for spinning continuous unidirectional sheets with tunable physical properties. *Nano Letters, 8*(2), 700-705.

[27] Li, Q. â., Zhang, X. â., DePaula, R. â., Zheng, L. â., Zhao, Y. â., Stan, L., . . . Zhu, Y. â. (2006). Sustained growth of ultralong carbon nanotube arrays for fiber spinning. *Advanced Materials, 18*(23), 3160-3163.

[28] Zhang, X., Li, Q., Holesinger, T. ?., Arendt, P. ?., Huang, J., Kirven, P. ?., . . . Zhu, Y. (2007). Ultrastrong, stiff, and lightweight carbon-nanotube fibers. *Advanced Materials, 19*(23), 4198-4201.

[29] Li, Y., Kinloch, I. A., & Windle, A. H. (2004). Direct spinning of carbon nanotube fibers from chemical vapor deposition synthesis. *Science, 304*(5668), 276-278.

[30] Vigolo, B., Pénicaud, A., Coulon, C., Sauder, C., Pailler, R., Journet, C., . . . Poulin, P. (2000). Macroscopic fibers and ribbons of oriented carbon nanotubes. *Science, 290*(5495), 1331-1334.

[31] Huynh, C. P., & Hawkins, S. C. (2010). Understanding the synthesis of directly spinnable carbon nanotube forests. *Carbon, 48*(4), 1105-1115.

[32] Zhang, X., Jiang, K., Feng, C., Liu, P., Zhang, L., Kong, J., . . . Fan, S. (2006). Spinning and processing continuous yarns from 4-inch wafer scale super-aligned carbon nanotube arrays. *Advanced Materials, 18*(12), 1505-1510.

[33] Fan, S., Chapline, M. G., Franklin, N. R., Tombler, T. W., Cassell, A. M., & Dai, H. (1999). Self-oriented regular arrays of carbon nanotubes and their field emission properties. *Science, 283*(5401), 512-514.

[34] Pöhls, J., Johnson, M. B., White, M. A., Malik, R., Ruff, B., Jayasinghe, C., . . . Shanov, V. (2012). Physical properties of carbon nanotube sheets drawn from nanotube arrays. *Carbon, 50*(11), 4175-4183.

[35] Atkinson, K. R., Hawkins, S. C., Huynh, C., Skourtis, C., Dai, J., Zhang, M., . . . Baughman, R. H. (2007). Multifunctional carbon nanotube yarns and transparent sheets: Fabrication, properties, and applications. *Physica B: Condensed Matter, 394*(2), 339-343.

[36] Wei, Y., Jiang, K., Feng, X., Liu, P., Liu, L., & Fan, S. (2007). Comparative studies of multiwalled carbon nanotube sheets before and after shrinking. *Phys.Rev.B, 76*(4), 045423.

[37] Aliev, A. E., Guthy, C., Zhang, M., Fang, S., Zakhidov, A. A., Fischer, J. E., & Baughman, R. H. (2007). Thermal transport in MWCNT sheets and yarns. *Carbon, 45*(15), 2880-2888.

[38] Prasher, R. S., Hu, X. J., Chalopin, Y., Mingo, N., Lofgreen, K., Volz, S., . . . Keblinski, P. (2009). Turning carbon nanotubes from exceptional heat conductors into insulators.

[39] Liu, B., Hsu, C., & Wang, W. (2012). A comparative study on preparation of conductive and transparent carbon nanotube thin films. *Journal of the Taiwan Institute of Chemical Engineers*, *43*(1), 147-152.

[40] Bädeker, K. (1907). Über die elektrische leitfähigkeit und die thermoelektrische kraft einiger schwermetallverbindungen. *Annalen Der Physik, 327*(4), 749-766.

[41] Radhakrishna, M., & Rao, M. (1977). Some properties of indium-tin oxide films. *Pramana, 9*(1), 1-6.

[42] Gordon, R. G. (2000). Criteria for choosing transparent conductors. *MRS Bulletin, 25*(08), 52-57.

[43] Minami, T. (2000). New n-type transparent conducting oxides. *MRS Bulletin, 25*(08), 38-44.

[44] Sheng, S., Fang, G., Li, C., Xu, S., & Zhao, X. (2006). p-type transparent conducting oxides. *Physica Status Solidi (a), 203*(8), 1891-1900.

[45] Neamen, D. A. (2003). *Semiconductor physics and devices : Basic principles*. Boston: McGraw-Hill.

[46] Lewis, B. G., & Paine, D. C. (2000). Applications and processing of transparent conducting oxides. *MRS Bulletin, 25*(08), 22-27.

[47] Kim, H., Gilmore, C. M., Piqué, A., Horwitz, J. S., Mattoussi, H., Murata, H., . . . Chrisey, D. B. (1999). Electrical, optical, and structural properties of indium–tin–oxide thin films for organic light-emitting devices. *Journal of Applied Physics, 86*(11), 6451-6461.

[48] Chiou, B., Hsieh, S., & Wu, W. (1994). Electrical behavior of low-power RF magnetron-sputtered indium tin oxide films on silicon substrate. *Applied Surface Science, 74*(4), 297-302.

[49] Mansingh, A., & Vasant Kumar, C. V. R. (1988). R.f.-sputtered indium tin oxide films on water-cooled substrates. *Thin Solid Films, 167*(1–2), L11-L14.

[50] Karulkar, P. C., & McCoy, M. E. (1981). D.C. magnetron sputter deposition of indium tin oxide films. *Thin Solid Films, 83*(2), 259-260.

[51] Wu, W., & Chiou, B. (1994). Properties of radio-frequency magnetron sputtered ITO films without in-situ substrate heating and post-deposition annealing. *Thin Solid Films, 247*(2), 201-207.

[52] Maki, K., Komiya, N., & Suzuki, A. (2003). Fabrication of thin films of ITO by aerosol CVD. *Thin Solid Films, 445*(2), 224-228.

[53] Zhou, Z. B., Cui, R. Q., Pang, Q. J., Wang, Y. D., Meng, F. Y., Sun, T. T., . . . Yu, X. B. (2001). Preparation of indium tin oxide films and doped tin oxide films by an ultrasonic spray CVD process. *Applied Surface Science, 172*(3–4), 245-252.

[54] Sawada, Y., Kobayashi, C., Seki, S., & Funakubo, H. (2002). Highly-conducting indium tin-oxide transparent films fabricated by spray CVD using ethanol solution of indium (III) chloride and tin (II) chloride. *Thin Solid Films, 409*(1), 46-50.

[55] Ohta, H., Orita, M., Hirano, M., Tanji, H., Kawazoe, H., & Hosono, H. (2000). Highly electrically conductive indium–tin–oxide thin films epitaxially grown on yttria-stabilized zirconia (100) by pulsed-laser deposition. *Applied Physics Letters, 76*(19), 2740-2742.

[56] Suzuki, A., Matsushita, T., Aoki, T., Mori, A., & Okuda, M. (2002). Highly conducting transparent indium tin oxide films prepared by pulsed laser deposition. *Thin Solid Films, 411*(1), 23-27.

[57] Izumi, H., Ishihara, T., Yoshioka, H., & Motoyama, M. (2002). Electrical properties of crystalline ITO films prepared at room temperature by pulsed laser deposition on plastic substrates. *Thin Solid Films, 411*(1), 32-35.

[58] Djaoued, Y., Vu Hong Phong, Badilescu, S., Ashrit, P. V., Girouard, F. E., & Vo-Van Truong. (1997). Sol-gel-prepared ITO films for electrochromic systems. *Thin Solid Films, 293*(1–2), 108-112.

[59] Mattox, D. M. (1991). Sol-gel derived, air-baked indium and tin oxide films. *Thin Solid Films, 204*(1), 25-32.

[60] Alam, M. J., & Cameron, D. C. (2000). Optical and electrical properties of transparent conductive ITO thin films deposited by sol–gel process. *Thin Solid Films, 377–378*(0), 455-459.

[61] Haacke, G. (1976). New figure of merit for transparent conductors. *Journal of Applied Physics, 47*(9), 4086-4089.

[62] Tolcin, A. (2012). Commodity statistics and information, non-fuel minerals: Indium. *U.S. Geological Survey*, , 74-75.

[63] Indium tin oxide and alternative transparent conductor markets (ref: Nano-096). (2009). *Focus on Powder Coatings, 2009*(6), 6-7.

[64] Ginley, D. S., & Bright, C. (2000). Transparent conducting oxides. *MRS Bulletin, 25*(08), 15-18.

[65] Wassei, J. K., & Kaner, R. B. (2010). Graphene, a promising transparent conductor. *Materials Today, 13*(3), 52-59.

[66] Niu, C., Sichel, E. K., Hoch, R., Moy, D., & Tennent, H. (1997). High power electrochemical capacitors based on carbon nanotube electrodes. *Applied Physics Letters, 70*(11), 1480-1482.

[67] Fu, K., & Sun, Y. (2003). Dispersion and solubilization of carbon nanotubes. *Journal of Nanoscience and Nanotechnology, 3*(5), 351-364.

[68] Ham, H. T., Choi, Y. S., & Chung, I. J. (2005). An explanation of dispersion states of single-walled carbon nanotubes in solvents and aqueous surfactant solutions using solubility parameters. *Journal of Colloid and Interface Science, 286*(1), 216-223.

[69] Vaisman, L., Wagner, H. D., & Marom, G. (2006). The role of surfactants in dispersion of carbon nanotubes. *Advances in Colloid and Interface Science, 128–130*(0), 37-46.

[70] Rastogi, R., Kaushal, R., Tripathi, S. K., Sharma, A. L., Kaur, I., & Bharadwaj, L. M. (2008). Comparative study of carbon nanotube dispersion using surfactants. *Journal of Colloid and Interface Science, 328*(2), 421-428.

[71] Niu, C. (2011). Carbon nanotube transparent conducting films. *MRS Bulletin, 36*(10), 766-773.

[72] Li, Z., Kandel, H. R., Dervishi, E., Saini, V., Xu, Y., Biris, A. R., . . . Biris, A. S. (2008). Comparative study on different carbon nanotube materials in terms of transparent conductive coatings. *Langmuir, 24*(6), 2655-2662.

[73] Hou, P., - Yu, B., - Su, Y., - Shi, C., - Zhang, L., - Liu, C., . . . - Cheng, H.- Double-wall carbon nanotube transparent conductive films with excellent performance The Royal Society of Chemistry.

[74] De, S., Lyons, P. E., Sorel, S., Doherty, E. M., King, P. J., Blau, W. J., . . . Coleman, J. N. (2009). Transparent, flexible, and highly conductive thin films based on Polymer Nanotube composites. *ACS Nano, 3*(3), 714-720.

[75] Wu, Z., Chen, Z., Du, X., Logan, J. M., Sippel, J., Nikolou, M., . . . Rinzler, A. G. (2004). Transparent, conductive carbon nanotube films. *Science, 305*(5688), 1273-1276.

[76] Saotome, T., Kim, H., Wang, Z., Lashmore, D., & Thomas Hahn, H. (2011). Transparent conducting film: Effect of vacuum filtration of carbon nanotube suspended in oleum. *Bulletin of Materials Science, 34*(4), 623-628.

[77] Fabrication and characterization of thin films of single-walled carbon nanotube bundles on flexible plastic substrates - American Chemical Society.

[78] Kaempgen, M., Duesberg, G. S., & Roth, S. (2005). Transparent carbon nanotube coatings. *Applied Surface Science, 252*(2), 425-429.

[79] Harutyunyan, A. R., Chen, G., Paronyan, T. M., Pigos, E. M., Kuznetsov, O. A., Hewaparakrama, K., . . . Sumanasekera, G. U. (2009). Preferential growth of single-walled carbon nanotubes with metallic conductivity. *Science}, 326*(5949), 116-120.

[80] Sundaram, R. M., Koziol, K. K. K., & Windle, A. H. (2011). Continuous direct spinning of fibers of single-walled carbon nanotubes with metallic chirality. *Advanced Materials, 23*(43), 5064-5068.

[81] Feng, C., Liu, K., Wu, J., Liu, L., Cheng, J., Zhang, Y., . . . Jiang, K. (2010). Flexible, stretchable, transparent conducting films made from superaligned carbon nanotubes. *Advanced Functional Materials, 20*(6), 885-891.

[82] Lin, H., Li, L., Ren, J., Cai, Z., Qiu, L., Yang, Z., & Peng, H. (2013). Conducting polymer composite film incorporated with aligned carbon nanotubes for transparent, flexible and efficient supercapacitor. *Sci.Rep., 3*

[83] Di, J., Hu, D., Chen, H., Yong, Z., Chen, M., Feng, Z., . . . Li, Q. (2012). Ultrastrong, foldable, and highly conductive carbon nanotube film. *ACS Nano, 6*(6), 5457-5464.

[84] Li, J., Hu, L., Wang, L., Zhou, Y., GrÃ¼ner, G., & Marks, T. J. (2006). Organic light-emitting diodes having carbon nanotube anodes. *Nano Letters, 6*(11), 2472-2477.

[85] Ago, H., Petritsch, K., Shaffer, M. S. P., Windle, A. H., & Friend, R. H. (1999). Composites of carbon nanotubes and conjugated polymers for photovoltaic devices. *Advanced Materials, 11*(15), 1281-1285.

[86] Gruner, G.- *Carbon nanotube films for transparent and plastic electronics* - The Royal Society of Chemistry.

[87] Valdes, L. B. (1954). Resistivity measurements on germanium for transistors. *Proceedings of the IRE, 42*(2), 420-427.

[88] Uhlir, A. (1955). The potentials of infinite systems of sources and numerical solutions of problems in semiconductor engineering. *Bell System Technical Journal, 34*(1), 105-128.

[89] Smits, F. M. (1958). Measurement of sheet resistivities with the four-point probe. *Bell System Technical Journal, 37*(3), 711-718

[90] Buehler, M. G., Shockley, W., & Pearson, G. L. (1964). Hall measurements using corbino-like current sources in thin circular disks. *Applied Physics Letters, 5*(11), 228-229.

[91] Buehler, M. G., & Pearson, G. L. (1966). Magnetoconductive correction factors for an isotropic hall plate with point sources. *Solid-State Electronics, 9*(5), 395-407.

[92] Swartzendruber, L. J. (1964). Four-point probe measurement of non-uniformities in semiconductor sheet resistivity. *Solid-State Electronics, 7*(6), 413-422.

[93] Buehler, M. G. (1967). A hall four-point probe on thin plates: Theory and experiment. *Solid-State Electronics, 10*(8), 801-812

[94] Topsoe, H. (1966). Geometric Factors in four point resistivity measurement. *Geometric Factors in four point resistivity measurement* (pp. 53-57)

[95] Chandrasekaran, C. (2012). Plastics calendering. *Handbook of troubleshooting plastics processes* (pp. 363-382) John Wiley & Sons, Inc.

[96] Schwenkner, S., & van Rüth, P. (2014). Innovative calendering technology for technical textiles. *Pakistan Textile Journal, 63*(2), 54.

[97] Forrest. (2004). The path to ubiquitous and low-cost organic electronic appliances on plastic. *Nature, 428*(6986), 911-918.

[98] Gyoujin Cho. (2010). All-printed and roll-to-roll-printable 13.56-MHz-operated 1-bit RF tag on plastic foils. *Electron Devices, IEEE Transactions on, 57*(3), 571-580.

[99] Lee, S., Nguyen, H. A. D., & Hoang, N. (2011). Application of calendering process to roll-to-roll printed electronics. *Advanced Materials Research, 317-318*, 436-439.

[100] Santa-Nokki, H., Kallioinen, J., Kololuoma, T., Tuboltsev, V., & Korppi-Tommola, J. (2006). Dynamic preparation of TiO2 films for fabrication of dye-sensitized solar cells. *Journal of Photochemistry and Photobiology A: Chemistry, 182*(2), 187-191.

[101] Hasegawa, K., & Noda, S. (2011). Millimeter-tall single-walled carbon nanotubes rapidly grown with and without water. *ACS Nano, 5*(2), 975-984.

[102] Amama, P. B., Pint, C. L., McJilton, L., Kim, S. M., Stach, E. A., Murray, P. T., . . . Maruyama, B. (2009). Role of water in super growth of single-walled carbon nanotube carpets. *Nano Letters, 9*(1), 44-49.

[103] Faraji, S., Stano, K., Rost, C., Maria, J., Zhu, Y., & Bradford, P. D. (2014). Structural annealing of carbon coated aligned multi-walled carbon nanotube sheets. Carbon, 79(0), 113-122.

[104] Chen, G., Futaba, D. N., Sakurai, S., Yumura, M., & Hata, K. (2014). Interplay of wall number and diameter on the electrical conductivity of carbon nanotube thin films. *Carbon, 67*(0), 318-325.

[105] Li, H. J., Lu, W. G., Li, J. J., Bai, X. D., & Gu, C. Z. (2005). Multichannel ballistic transport in multiwall carbon nanotubes. *Phys.Rev.Lett.*, *95*(8), 086601.

[106] Li, Z., Kandel, H. R., Dervishi, E., Saini, V., Biris, A. S., Biris, A. R., & Lupu, D. (2007). Does the wall number of carbon nanotubes matter as conductive transparent material? *Applied Physics Letters*, *91*(5)

[107] Souza Filho, A.G., Jorio, A., Samsonidze, G., Dresselhaus, M.S., & Saito, R. (2003). Raman spectroscopy for probing chemically/physically induced phenomena in carbon nanotubes. *Nanotechnology*, *14*(10), 1130.

[108] Vix-Guterl, C., Couzi, M., Dentzer, J., Trinquecoste, M., & Delhaes, P. (2004). Surface characterizations of carbon multiwall nanotubes: Comparison between surface active sites and raman spectroscopy. *The Journal of Physical Chemistry B, 108*(50), 19361-19367

[109] Kaskela, A., Nasibulin, A. G., Timmermans, M. Y., Aitchison, B., Papadimitratos, A., Tian, Y., . . . Kauppinen, E. I. (2010). Aerosol-synthesized SWCNT networks with tunable conductivity and transparency by a dry transfer technique. *Nano Letters*, *10*(11), 4349-4355.

[110] Shin, D.W., Lee, J.H., Kim, Y.H., Yu, S.M., & Park, S.Y. (2009). A role of HNO3 on transparent conducting film with single-walled carbon nanotubes. *Nanotechnology, 20*(47), 475703

[111] Geng, H., Kim, K. K., So, K. P., Lee, Y. S., Chang, Y., & Lee, Y. H. (2007). Effect of acid treatment on carbon nanotube-based flexible transparent conducting films.*Journal of the American Chemical Society*, *129*(25), 7758-7759.

[112] Loyola, B. R., Zhao, Y., Loh, K. J., & La Saponara, V. (2012). The electrical response of carbon nanotube-based thin film sensors subjected to mechanical and environmental effects. *Smart Materials and Structures, 22*(2), 025010-1-11.

[113] Park, M., Kim, H., Youngblood, J.P. (2008). Strain-dependent electrical resistanec of multi-walled carbon nanotube/polymer composite films. *Nanotechnology*, *19*(5), 055705

[114] Song, X., Liu, S., Gan, Z., Lv, Q., Cao, H., & Yan, H. (2009). Controllable fabrication of carbon nanotube-polymer hybrid thin film for strain sensing. *Microelectronic Engineering, 86*(11), 2330-2333.

[115] Hu, N., Karube, Y., Yan, C., Masuda, Z., & Fukunaga, H. (2008). Tunneling effect in a polymer/carbon nanotube nanocomposite strain sensor. *Acta Materialia*,*56*(13), 2929-2936.

[116] Yoon, Y., Song, J., Kim, D., Kim, J., Park, J., Oh, S., & Han, C. -. (2007). Transparent film heater using single-walled carbon nanotubes. *Advanced Materials*, *19*(23), 4284-4287.

[117] Jung, D., Kim, D., Lee, K. H., Overzet, L. J., & Lee, G. S. (2013). Transparent film heaters using multi-walled carbon nanotube sheets. *Sensors and Actuators A: Physical*, *199*(0), 176-180.

[118] Jang, H., Jeon, S. K., & Nahm, S. H. (2011). The manufacture of a transparent film heater by spinning multi-walled carbon nanotubes. *Carbon*, *49*(1), 111-116.

APPENDICES

Appendix A

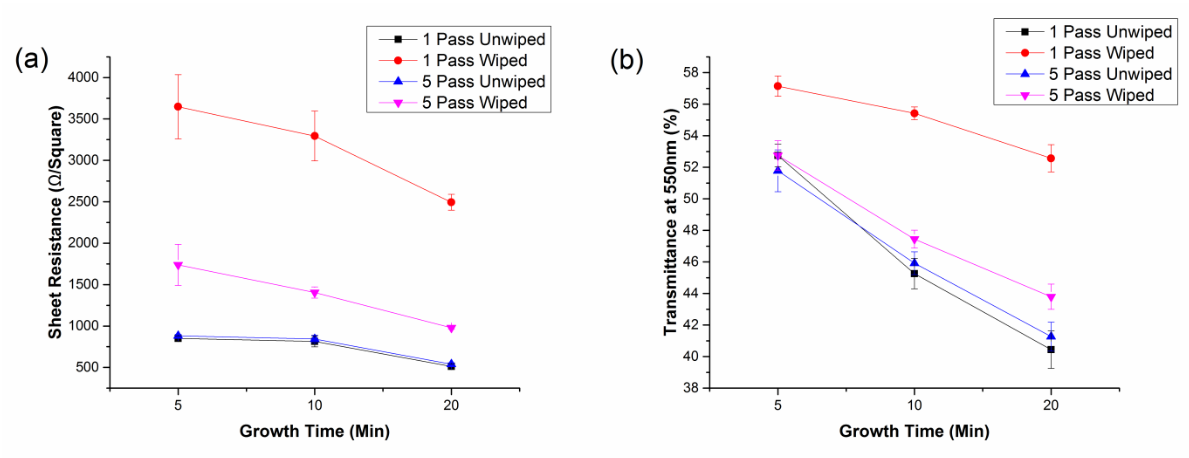

Figure A.1 (a) Sheet resistance and (b) transmittance of CNTs with variable growth times grown with original growth setup using an argon/chlorine mixture..